Journal of Medicinal Chemistry

Article

Hydroxamic acid inhibitors provide cross-species inhibition of Plasmodium M1 and M17 aminopeptidases.

Natalie B Vinh, Nyssa Drinkwater, Tess R Malcolm, Michael Kassiou, Leonardo Lucantoni, Peter M Grin, Georgina S Butler, Sandra Duffy, Christopher M Overall, Vicky M. Avery, Peter J. Scammells, and Sheena McGowan

J. Med. Chem., **Just Accepted Manuscript** • DOI: 10.1021/acs.jmedchem.8b01310 • Publication Date (Web): 11 Dec 2018

Just Accepted

ACS Publications

is published by the American Chemical Society. 1155 Sixteenth Street N.W., Washington, DC 20036

Hydroxamic acid inhibitors provide cross-species inhibition of *Plasmodium* M1 and M17 aminopeptidases

Natalie B. Vinh [a,§], Nyssa Drinkwater [b,§], Tess R Malcolm [b], Michael Kassiou,[c] Leonardo Lucantoni [d], Peter M Grin [e], Georgina S Butler [e,f], Sandra Duffy [d], Christopher M Overall [e,f], Vicky M. Avery [d], Peter J. Scammells [a,*], Sheena McGowan [b,*]

[a] Medicinal Chemistry Monash Institute of Pharmaceutical Sciences, Monash University Parkville, Melbourne, VIC 3052, Australia.

[b] Biomedicine Discovery Institute, Department of Microbiology, Monash University, Clayton, Melbourne, VIC 3800, Australia.

[c] School of Chemistry, University of Sydney, NSW 2006, Australia

[d] Discovery Biology, Griffith Institute for Drug Discovery, Griffith University, Nathan, Queensland 4111, Australia.

[e] Centre for Blood Research, Department of Biochemistry & Molecular Biology, University of British Columbia, Vancouver, British Columbia V6T 1Z3, Canada

[f] Centre for Blood Research, Department of Oral Biological and Medical Sciences, University of British Columbia, Vancouver, British Columbia V6T 1Z3, Canada

KEYWORDS: falciparum malaria, vivax malaria, aminopeptidase, inhibitors, hydroxamic acid, metallo-proteins

ABSTRACT: There is an urgent clinical need for antimalarial compounds that target malaria caused by both *Plasmodium falciparum* and *Plasmodium vivax*. The M1 and M17 metalloexopeptidases play key roles in *Plasmodium* haemoglobin digestion, and are validated drug targets. We used a multi-target strategy to rationally design inhibitors capable of potent inhibition of the M1 and M17 aminopeptidases from both *P. falciparum* (*Pf*-M1 and *Pf*-M17) and *P. vivax* (*Pv*-M1 and *Pv*-M17). The novel chemical series contains a hydroxamic acid zinc binding group to coordinate catalytic zinc ion/s, and a variety of hydrophobic groups to probe the S1' pockets of the four target enzymes. Structural characterisation by co-crystallisation showed that selected compounds utilise new and unexpected binding modes; most notably, compounds substituted with bulky hydrophobic substituents displace the *Pf*-M17 catalytic zinc ion. Excitingly, key compounds of the series potently inhibit all four molecular targets and show antimalarial activity comparable to current clinical candidates.

■ INTRODUCTION

Malaria is a widespread parasitic disease; half of the world's population, equating to approximately 3.2 billion people, is at risk of contracting malaria. In 2016, an estimated 216 million people contracted malaria and 445,000 deaths were reported.[1] Malaria is caused by five species of the *Plasmodium* genus: *Plasmodium falciparum, Plasmodium malariae, Plasmodium ovale, Plasmodium vivax* and *Plasmodium knowlesi. P. falciparum* is responsible for an estimated 90% of malaria deaths worldwide, making it the most severe and lethal form of the disease[1]; however, *P. vivax*, which is the predominant parasite causing human malaria outside of Africa, also causes substantial morbidity, primarily due to the difficulty obtaining a complete cure, which results in disease recurrence.[2] Efforts to control malaria and prevent its spread to new regions have been hindered by the emergence of drug resistance, including to artemisinin, our last line of defense.[3, 4] Despite the global health toll of malaria, the widespread resistance to commonly used antimalarials, and the alarming development of artemisinin resistance, there are few novel therapeutics in the pipeline. Further, many of the treatments in the Medicine for Malaria Venture (MMV) pipeline, the major source of new antimalarial therapeutics, still contain artemisinin or its derivatives. Therefore, new therapeutics with novel mechanisms of action and activity against both *P. falciparum* and *P. vivax* are urgently required.

Hemoglobin digestion is an essential metabolic process in the intra-erythrocytic stage of the *Plasmodium* life cycle. During this process, malaria parasites digest up to 75% of host cell hemoglobin resulting in the liberation of amino acids required for parasite protein synthesis.[5, 6] Two zinc-dependent metalloaminopeptidases, *Pf*-M1 and *Pf*-M17, are involved in the latter stages of hemoglobin degradation (Supplementary Figure 1), and are essential for parasite survival.[7-9] *In vitro* studies have shown that *Pf*-M1 inhibition kills the parasites by preventing proteolysis of hemoglobin peptides, whilst *Pf*-M17 inhibition kills the parasites earlier in the life cycle, suggestive of an additional role for *Pf*-M17 beyond hemoglobin digestion.[7] Further, inhibition of both aminopeptidases *in vivo* reduced parasitemia in *Plasmodium chabaudi chabaudi* murine models of

malaria.[10, 11] As such, *Pf*-M1 and *Pf*-M17 are validated targets for antimalarial therapy, and have been targeted in a variety of drug discovery programs.[10-22]

Pf-M1 and *Pf*-M17 both use a zinc (Zn^{2+})-dependent mechanism to hydrolyze the scissile peptide bond to catalyse the removal of single amino acids from the N-terminus of short peptides. Despite performing near-identical reactions, albeit with distinct specificities for the amino acid residue they remove (P1 position),[23] the enzymes themselves are from different enzyme families and possess very different three-dimensional structures.[24, 25] *Pf*-M1 is a monomeric protein of four domains, and has an active site containing a single catalytic Zn^{2+} ion buried deep within the catalytic domain.[25] *Pf*-M17 is a homo-hexameric protein, with each subunit comprised of two domains. The six active sites of the *Pf*-M17 hexamer each contain two catalytic Zn^{2+} ions, and lie on the edge of catalytic domains where they are exposed to the large internal cavity of the hexamer.[24] Despite these differences, the active sites of *Pf*-M1 and *Pf*-M17 share a similar structural arrangement; both possess S1 and S1' pockets (to accommodate substrate P1 and P1' residues), with bound Zn^{2+} ion/s at the junction of the two sub-sites.[24, 25] These common features led us to propose that, through rational drug design, we could develop a single compound capable of potent, dual inhibition of both *Pf*-M1 and *Pf*-M17, an attractive strategy for slowing the development of drug resistant parasites.[17, 20]

Research within our group has used rational drug discovery to optimise arginine mimetics into potent dual *Pf*-M1 and *Pf*-M17 inhibitors (Supplementary Figure 2).[15, 17, 20] *N*-(2-(Hydroxyamino)-2-oxo-1-(3',4',5'-trifluoro-[1,1'-biphenyl]-4-yl)ethyl)pivalamide (**1**) coordinates the catalytic Zn^{2+} ion/s through a hydroxamic acid moiety, and occupies the S1 and S1' pockets of both enzymes with the trifluoro-biphenyl and pivalamide moieties, respectively (Supplementary Figure 3).[15] In the S1 pocket of *Pf*-M1, the fluorine substituents interact through an intricate network of water-mediated hydrogen bonds, whilst in *Pf*-M17, the trifluorophenyl ring binds solely through hydrophobic interactions with neighboring Leu492, Phe583 and Met392 residues. Having optimized the binding interactions within the S1 pockets of both enzymes, we sought to improve

the pivalamide portion of the molecule, which binds the S1' pocket. Further, we elected to extend our strategy to target the M1 and M17 homologs in *P. vivax* (*Pv*-M1 and *Pv*-M17) to expand the capacity of our lead compounds and develop cross-species therapeutics.

■ RESULTS

Multi-target inhibition strategy. To achieve effective cross-species activity against *P. falciparum* and *P. vivax* by dual inhibition of M1 and M17, compounds capable of potent inhibition of all four molecular targets are required. The challenge this multi-target strategy presents to rational drug design is lessened by the high degree of sequence conservation between the *Plasmodium* homologs. The M1 homologs of *P. falciparum* and *P. vivax* share 72% sequence identity (89% within catalytic domains), while the M17 homologs share 70% identity (92% catalytic domains). Furthermore, the inhibitor binding residues are highly conserved; based on the previously determined crystal structures of *Pf*-M1 and *Pf*-M17 in complex with **1**, the residues lining the active sites and interacting with the inhibitors are 100% conserved between the cross-species homologs. Given this sequence conservation, and the highly conserved reaction mechanisms utilized by the M1 and M17 aminopeptidase families, it is likely that the structure of the active sites is also highly conserved across species. To investigate if these similarities would allow for cross-species inhibition by our inhibitors, we produced recombinant *Pv*-M1 and *Pv*-M17. The *Pv*-M1 (residues 195–1097) and *Pv*-M17 (residues 203–621) protein constructs were designed and produced in line with methods used for the *Pf* homologs, and demonstrated comparable kinetic parameters against the reporter substrate, L-leucine-7-amido-4-methylcoumarin, in our fluorescence-based assay system (complete biochemical characterization of *Pv*-M1 and *Pv*-M17 to be reported elsewhere). Interestingly, we found that **1**, designed to target the *Pf* enzymes, is actually more potent against the *Pv* enzymes (Table 1). This result supports the assertion that the structures of each of the M1 and M17 active sites are highly conserved between *Pf* and *Pv*. We therefore elected to perform further rational design of inhibitors targeting the M1 and M17 aminopeptidases

from both *P. falciparum* and *P. vivax* (four total targets), guided by structural analysis of the *Pf* enzymes.

Chemical synthesis of S1' exploratory series. Changes to the amide functionality of **1** were made to optimize interactions in the S1' pockets of *Pf*-M1/*Pf*-M17 thereby enhancing binding and inhibitory potency. A series of hydroxamic acid analogues containing hydrophobic groups that vary in size and shape were explored to investigate which groups could best satisfy the S1' pockets of the four target enzymes. Different hydrophobic groups were incorporated into the scaffold using a four-step reaction sequence shown in Scheme 1. Briefly, 2-amino-2-(4-bromophenyl)acetic acid (**2**) was esterified using standard conditions. The resultant methyl ester **3** was further functionalized using a Suzuki reaction to append the 3,4,5-trifluorophenyl ring. A mixture of compound **3**, 3,4,5-trifluorophenylboronic acid, $PdCl_2(PPh_3)_2$, $Na_2CO_{3\ (aq)}$ and THF was refluxed for 2 hours to give the key amine intermediate **4** in good yield (65%). The amine **4** was then elaborated with the desired hydrophobic substituent by treatment with either an acid chloride or an acid in the presence of peptide coupling reagents. These reactions proceeded in moderate yields (28–85%) with the exception of the 2,2,3,3,3-pentafluoropropanamide analogue **5e**, which was obtained in poor yield (7%) when HCTU was used as the coupling reagent. A small improvement in yield (42%) was observed when EDC.HCl was used. Finally, aminolysis of the methyl esters **5a-5r** with hydroxylamine hydrochloride and potassium hydroxide in anhydrous methanol gave the hydroxamic acid analogues (**6a-6r**) in low to good yields (22–75%).

Compound series inhibits multiple targets. Previous examination of the activity of *Pf*-M1[25] and *Pf*-M17[26] utilized a fluorescence-based assay system to monitor cleavage of the commercially available reporter substrate L-leucine-7-amido-4-methylcoumarin. We have previously adapted this system to examine inhibition of both *Pf*-M1 and *Pf*-M17 by calculation of compound inhibition constants (K_i) using the Dixon method. During the examination of the current series of compounds, we determined that compounds were inhibiting the enzymes with inhibition constants below the

concentration of enzyme in the assay. We therefore re-structured our method of compound examination to use a modified Morrison equation for tight-binding inhibitors and performed all assays in biological triplicate.[27, 28] This alteration in methodology resulted in a small discrepancy between the K_i values of compound **1** reported here (K_i *Pf*-M1 = 331 nM, K_i *Pf*-M17 = 147 nM) and that reported previously (K_i *Pf*-M1 = 80 nM, K_i *Pf*-M17 = 60 nM).[15] The methods utilised herein provide a robust method to evaluate tight-binding inhibitors against four different molecular targets, and we recommend they be used to assess all inhibitors of the *Plasmodium* aminopeptidases in future studies. We determined the inhibitory activity of **6a-r** against the M1 and M17 enzymes from both *P. falciparum* and *P. vivax*. The binding affinities (K_i) of the synthesized compounds to all four enzymes are described in Table 1. The rational design of compound/s capable of potent inhibition of four different enzymes presents a number of logistical difficulties. To simplify, we elected to analyze trends in the binding potencies first between homologous enzyme pairs (*Pf- vs Pv*-M1 and *Pf- vs Pv*-M17), and then between enzyme families (M1 *vs* M17).

Overall, the compound series inhibits *Pv*-M1 with approximately 10-fold greater affinity than *Pf*-M1, demonstrating that key differences between the M1 homologs exist that have a profound influence on compound binding and inhibition (Figure 1A, Table 1). Despite the difference in affinities, the trends in potency within the series are largely conserved, that is, the most potent inhibitors of *Pv*-M1 are also the most potent *Pf*-M1 inhibitors (Figure 1A). Analogs of **1** that lack one or two methyl groups of the pivalamide (compounds **6a** and **6b**, respectively) displayed significantly lower M1 binding affinity. A small series of fluorine-containing *tert*-butyl isosteres (compounds **6c-e**) were also evaluated. Of these compounds, only one diastereomer of the 2,3,3,3-tetrafluoropropanamide **6d** (**6d-a**) inhibited both the *Pf*-M1 and *Pv*-M1 enzymes with comparable potency to **1**. A series of cycloalkylcarboxamides was also prepared and assessed (compounds **6f-k**) to further define the steric requirements for optimal *Pf*-M1 and *Pv*-M1 activity. The cyclobutyl- and cyclopentylcarboxamides (**6g** and **6h**, respectively) proved to be the most potent inhibitors of both enzymes, while analogs of smaller ring size (cyclopropyl; **6f**) or larger ring size (cyclohexyl; **6i**)

were significantly less potent inhibitors of both *Pf*-M1 and *Pv*-M1. Interestingly, the adamantyl carboxamide **6k** inhibited *Pf*-M1 with higher potency (*Pf*-M1 K_i = 137 nM) than **1**, but was a much weaker inhibitor (K_i = 122 nM) than **1** at *Pv*-M1.

Extension of the carboxamide of **1** by one methylene unit in the 3,3-dimethylbutanamide analog **6l** improved potency at both enzymes (*cf.* *Pf*-M1 = 269 nM, *Pv*-M1 = 6.39 nM). Based on this promising finding, a series of cycloalkyl acetamides which possessed an analogous methylene spacer between the amide carbonyl and the cycloalkyl moiety (compounds **6m-p**) were prepared and evaluated. This series was generally more potent than the corresponding cycloalkyl carboxamides which lacked the methylene spacer (i.e. compounds **6f-i**), with the exception of the cyclohexyl analogs **6i** and **6p**, which were equipotent. In terms of compounds **6m-p**, the cyclobutylacetamide **6n** was the most potent inhibitor of *Pf*-M1 (K_i = 177 nM), with both the cyclopropyl and cyclopentylacetamides exhibiting slightly lower potency (**6m**; K_i = 202 nM and **6o**; K_i = 216 nM, respectively). The same general trend was observed at the *Pv*-M1 enzyme, where the cyclobutylacetamide **6n** was once again proved to be the most potent (*Pv*-M1 K_i = 2.85 nM), with reduced potency observed for the cyclopropyl and cyclopentylacetamides (**6m**; K_i = 17.9 nM and **6o**; K_i = 7.58 nM, respectively). In order to further probe the steric requirements of the S1'-binding pocket the fused cycloalkyl groups **6q** and **6r** were assessed. Both the cubanylacetamide **6q** and the norbornylacetamide **6r** exhibited potent inhibitory activity at both *Pf* and *Pv*-M1 enzymes, with **6q** proving to be the most potent M1 inhibitor of all compounds studied (K_i *Pf*-M1 = 88.9 nM, *Pv*-M1 = 1.73 nM).

Determination of the binding potencies of **6a-r** for *Pf*- and *Pv*-M17 shows that, unlike the M1 enzymes, the scale of inhibition of **6a-r** is largely conserved between the two M17 homologs (Figure 1B and Table 1). Analysis of the trends in inhibition potency across the series highlights some interesting similarities and differences between M17 homologs. The changes to binding potency of the alkyl, fluoroalkyl and cycloalkyl carboxamides **6a-k** are conserved between the two M17 enzymes (Figure 1B and Table 1). Of analogs **6a-k**, only one produced stronger inhibition of

Pf- and *Pv*-M17 compared to **1**. Compound **6k**, containing a bulky hydrophobic adamantyl moiety, showed the most potent inhibition of *Pf*-M17 observed to date (K_i = 28.9 nM) as well as highly potent *Pv*-M17 inhibition (K_i = 18.6 nM).

Incorporation of a methylene spacer adjacent to the carboxamide resulted in substantial divergence between the *Pf* and *Pv* homologs (**6l-6r**, Figure 1B, Table 1). There is clearly a difference in the capacity of the S1' pockets of *Pf*- and *Pv*-M17 to accommodate hydrophobic moieties. In general, the derivatives **6l-r** showed stronger inhibition of the *Pv*-M17 homolog versus the *Pf*-M17 homolog with exception of compounds **6m** and **6o**. Binding affinity of compounds **6l-p** to *Pf*- and *Pv*-M17 largely improved relative to their analogous compound without the methylene unit (**1**, **6f-i**). The 3,3-dimethylbutanamide **6l** proved to be the most potent inhibitor at both *Pf*- and *Pv*-M17 with K_i values of 101 and 3.60 nM, respectively. Interestingly there was no clear correlation between the size of the carboxamide and inhibitory activity across this series. Of the fused cycloalkylacetamides **6q** and **6r**, norbonylacetamide **6r** was equivalent in inhibitory potency to both M17 enzymes (K_i *Pf*-M17 = 127 nM, *Pv*-M17 = 93.1 nM) compared to **1**.

Overall, both the M1 and M17 enzymes from *Pf* and *Pv* were able to accommodate a number of different hydrophobic groups. While the binding capacity of the series showed substantial variation between the four enzymes, the cycloalkyl acetamides (compounds **6m-p**) were generally the most potent multi-target inhibitors of the series, with all but **6p**, demonstrating potent inhibition of all four enzymes. These results indicate that it is possible to develop a single compound capable of potent inhibition of both the M1 and M17 aminopeptidases across multiple *Plasmodium* species.

Binding mode of selected lead compounds to *Pf*-M1. To support the SAR data, and to inform further rational design, we determined the crystal structures of *Pf*-M1 with selected compounds of the series (Supplementary Table 1 and 2). The eight structures all showed clear compound density for the compounds in the *Pf*-M1 active site, with all of the compounds coordinating the catalytic Zn^{2+} through the hydroxamic acid. Further, the conserved trifluoro-biphenyl substituents all adopt identical poses in the S1 site, as was observed on binding of

compound **1** previously.[15] The overall quaternary structure of *Pf*-M1 is also largely conserved. When compared to the unliganded *Pf*-M1 structure, a small shift (0.5 Å) in the backbone of residues 319–Thr321, which sits just behind the S1 site, is observed, with Glu319–Ala320 adopts the cis-configuration in all eight structures described herein.

The lack of distinct inhibition trend across the *Pf*-M1 series was curious, in that the most potent compounds were substituted with mid-size (*tert*-butyl to cyclopentyl) or large (e.g. cubanyl) hydrophobic moieties. We were particularly interested to determine why all three of the compounds substituted with six-membered rings (**6i**, **6j**, and **6p**) were relatively weak inhibitors compared to the closely related five-membered ring analogs (**6h** and **6o**). The parent compound **1** coordinates the catalytic Zn^{2+} through the hydroxamic acid, which orients the carboxamide to allow the hydrophobic *tert*-butyl moiety access to the S1' site wherein it forms interactions with the pi electrons of His496, and hydrophobic interactions with Tyr580 and Val493 (Supplementary figure 3A).[15] The carboxamide itself also forms key hydrogen bonds with the backbone amine of Gly460 and Ala461.[15] The crystal structure of *Pf*-M1 in complex with **6h** (1.35 Å) shows that the cyclopentyl moiety of **6h** largely occupies the same space as the *tert*-butyl moiety of **1**, but forms closer interactions with Val493 and the pi cloud of His496 (Figure 2A), which accounts for the modest improvement in inhibitor potency. These interactions are optimized further in the cyclopentylacetamide **6o**, which combines the cyclopentyl moiety with a methylene spacer. *Pf*-M1:**6o** (determined to 1.5 Å) demonstrates that this extension allows the cyclopentane ring deeper access into the S1' pocket where it forms hydrophobic interactions of an ideal length with Val493 and Thr492, while also maintaining the interactions with the zinc-binding residue His496 (Figure 2B). The improvement in binding of **6o** compared to **6h** is only modest (K_i = 216 nM compared to 285 nM), which is likely due to the closer unfavorable contacts with Arg489 formed by **6o**. Any additional steric bulk in this position would be more unfavorable, which likely indicates why the cyclohexane-substituted analogues are poor inhibitors. To confirm, we determined the structure of *Pf*-M1 in complex with cyclohexylcarboxamide **6i** and cyclohexylacetamide **6p** to 1.65 Å and 1.50

Å respectively. The cyclohexyl group of **6i** sits within the S1' pocket, and as predicted, clashes with Arg489. Additionally, the adopted conformation is high energy; substituent is axial and the ring adopts a strained chair conformation, with C1–C2–C3 angle of 98°. Together, these observations account for the weak binding of **6i**. Surprisingly, the added methylene spacer of **6p** results in a drastically altered *Pf*-M1 binding conformation. The cyclohexyl substituent has moved out of the S1' pocket, and instead occupies the substrate/product access channel (Figure 2C). This rearrangement likely occurred to avoid steric clashes of the bulker substituent with the spatially limited S1' pocket. Unfortunately, the new binding mode places the cyclohexyl substituent within a solvated environment, and offers few binding options for a hydrophobic moiety, and as a consequence, reduces binding potency. The ring interacts with the face of Tyr580 (Figure 2D), but this proximity also results in close contact between the ring of **6p** and the backbone carbonyl of Tyr575, which results in local small-scale rearrangement of the protein chain similar to that observed on binding of other large inhibitors.[29] Further, the change in carboxamide geometry required to elicit the new binding mode resulted in a lengthening of the hydrogen bond between carbonyl oxygen and backbone amine of Gly460 and loss of the hydrogen bond to Ala461 (Figure 2B compared to 2D). We also examined the binding of the cyclopropylacetamide **6m**. Interestingly, the structure of *Pf*-M1:**6m** (1.58 Å) showed that the cyclopropane ring of **6m** also occupies the access channel rather than the S1' site similar to **6p**. The contrasting conformational preference of **6m** compared to **6o** indicates both substituent geometry as well as size influences the *Pf*-M1 binding mode. Despite occupying the access channel rather than the S1' subsite, **6m** does not suffer the same loss of potency as **6p**. This is likely because the smaller **6m** does not cause the Tyr575 backbone re-arrangement observed on binding **6p**, nor require the change in geometry of the N-acyl group. Together, these observations account for the loss of potency observed for **6p** compared to **6l-6n**.

Having accounted for the loss of potency of compounds substituted with a 6-membered ring, we questioned how the larger **6k**, **6q** and **6r** regained affinity to possess the tightest *Pf*-M1

inhibition constants of the series. We therefore determined the structure of *Pf*-M1 in complex with **6k**. Despite high resolution (1.82 Å), the electron density for the adamantyl moiety was highly disordered. Whilst we were able to model the substituent at partial occupancy (50%) placed mid-way between the S1' subsite and the access channel, the structure provided limited insight into additional interactions that may be gained by these large hydrophobic groups.

Finally, we sought to investigate the structural mechanism by which *Pf*-M1 discriminates between the diastereomers, **6d-a** and **6d-b**. We therefore determined the crystal structure of **6d-a**, in complex with *Pf*-M1 (1.81 Å). Electron density clearly indicated that the inhibitor molecule in complex with the enzyme has the *R*,*R*-configuration. This structure showed that the hydroxamic acid zinc binding group and biphenyl system of **6d-a** bind *Pf*-M1 comparably to the parent compound **1**. The interactions of the carboxamides are comparable, as are as the interactions with the face of His496 formed by both pivalamide of **1** and the 2,3,3,3-tetrafluoropropanamide **6d-a**. Within the S1' pocket, the dual natured 2,3,3,3-tetrafluoropropanamide is able to form interactions with the face of His496 and Val493 (similarly to **1**), as well as additional interactions with Arg489 (unfavourable to **1**), which likely accounts for the tighter binding of **6d-a**.

Binding mode of selected lead compounds to *Pf*-M17. Inhibition data determined that insertion of a methylene spacer to bulky hydrophobic substituents was generally favorable for binding *Pf*-M17. We therefore elected to determine the crystal structures of *Pf*-M17 in complex with **6k**, the most potent *Pf*-M17 inhibitor of the series. The first round of crystallization experiments yielded unexpected results; **6k** uses a novel zinc-binding mode to inhibit *Pf*-M17 via a previously unobserved mechanism. M17 aminopeptidases possess a conserved binuclear metal center containing 'catalytic' and 'regulatory' metal binding sites.[30] Full activity requires both sites to be occupied; however the regulatory metal ion is readily lost in crystal structures.[24, 31] Untreated *Pf*-M17 crystals have only the 'catalytic' Zn^{2+} bound (Figure 3A), and require treating with a Zn^{2+} soak solution to occupy both sites and achieve the 'active' form of the enzyme used for inhibitor design (Figure 3B). Using these methods, we previously determined the parent compound **1** binds

to *Pf*-M17 by coordinating both Zn^{2+} ions, a conformation that is repeated in all *Pf*-M17 active sites (two copies of the *Pf*-M17 hexamer in the asymmetric unit afford 12 total views of the active site) (Figure 3C).[15] However, use of identical co-crystal growth and Zn^{2+} treatment methods to determine *Pf*-M17:**6k** yielded an unliganded structure, and increasing the concentration of **6k** in the Zn^{2+} soak solution yielded only very weak density for the compound. Given the potent inhibition of *Pf*-M17 by **6k**, the difficulty obtaining a co-crystal structure was puzzling. We collected a final dataset to 2.30 Å from a co-crystal that was not treated with additional Zn^{2+}; the structure showed clear electron density for **6k** and only a single Zn^{2+}. Surprisingly, the single Zn^{2+} occupies the 'regulatory' site, indicating that the 'catalytic' Zn^{2+} site cannot be occupied whilst **6k** is bound (Figure 3D). Such an active site arrangement, wherein the 'catalytic' site is unoccupied, has not been observed in any other structure of M17 aminopeptidases. To determine whether Zn^{2+} displacement was a consequence of the large hydrophobic substituent on **6k** or characteristic of other compounds in the series, we also determined the structure of *Pf*-M17 in complex with **6i** (2.10 Å), which with a cyclohexane substituted off the N-acyl is intermediate in size between **1** and **6k**, and retains tight binding capability. With the exception of the compound identity, the crystal was treated identically to that which yielded *Pf*-M17:**1** (including a Zn^{2+} soak step). In the *Pf*-M17:**6i** structure, clear electron density was observed for the compound, however the electron density in the catalytic Zn^{2+} site was weak, and not indicative of a metal ion. Although it is possible the Zn^{2+} is at low occupancy, it could not be modeled. It was therefore clear that **6i** was also in competition with the catalytic Zn^{2+}.

Beyond the unexpected displacement of the catalytic Zn^{2+} ion, the interactions between *Pf*-M17 and **6i**/**6k** were largely as expected. The binding position of the hydroxamic acid has shifted slightly compared to that of the parent compound **1** (Figure 4A). This is likely the result of the bulky substituents occupying the S1' pocket, and the cause of the Zn^{2+} displacement. In place of metallo-bonds, the hydroxyl of **6i** and **6k** form hydrogen bonds with Glu461 and Lys374, and the catalytic carbonate ion (Figure 4B). Despite the large variation in mechanism of Zn^{2+} coordination,

the change has little effect on the compound binding position. Similarly to **1** (Supplementary Figure 3B), the trifluoro-substituted biphenyl system occupies the S1 pocket (Figure 4A), where it forms the same hydrophobic interactions. The large S1' subsite of *Pf*-M17 was able to accommodate the bulky hydrophobic substituents, wherein they interact with Ala460, Ile547, and the aliphatic chain of Ser554 (Figure 4B). Of particular note is that the bulky groups form unfavorably close contacts with Asn457 (Figure 4B), which is spatially restricted and unable to move away from the contact. We predict it is these contacts that cause the shift in binding position of the N-acyl linker and hydroxamic acid, which results in displacement of the catalytic Zn^{2+}. Alternatively, the large hydrophobic substituents may be altering the environment of the pocket to destabilize the charged Zn^{2+}; however it is unknown why the catalytic Zn^{2+}, rather than the regulatory Zn^{2+}, which is spatially closer to the hydrophobic moiety and previously shown to be readily lost from the active site, would be affected.

Binding of 6k is partially reversible. We performed washout experiments to determine whether binding of **6k**, which displaces the catalytic Zn^{2+}, is reversible. We treated the enzyme with either EDTA, **6k**, or bestatin (competitive substrate-analogue inhibitor), washed the protein with metal-free buffer, and then monitored the time-dependent activity on addition of metal cofactor and substrate (Supplementary Figure 4). A short buffer exchange (2 hours) was sufficient to recover the activity of EDTA treated *Pf*-M17. However, longer wash steps were required to completely remove bestatin (normal activity of bestatin-treated *Pf*-M17 was observed after a 5 hour wash). In contrast, after the 5-hour wash, only minimal activity was observed in the *Pf*-M17 sample treated with compound **6k**. Further washing recovered more of the activity, but after 7 hours of buffer exchange, only approximately 20% of activity was recovered in the **6k**-treated *Pf*-M17 sample. Therefore, while **6k**-treatment appears to be reversible, it likely requires long wash times to recover activity. Since EDTA-treated enzyme recovers quickly, the slow recovery of the **6k**-treated sample is likely a result of a slow compound off-rate rather than metal removal.

Anti-parasitic activity of key compounds. We have previously shown that **1** potently inhibits *P. falciparum* growth *in vitro*, including the multi-drug resistant strain Dd2.[32] We triaged the current compound series for assessment in an *in vitro P. falciparum* phenotypic assay by selecting only those compounds that demonstrated potent dual *Pf*-M1 and *Pf*-M17 inhibitory capability ($K_i \leq 200$ nM against one *Pf* target, and ≤ 400 nM against the second). The compounds were tested against both drug-resistant (Dd2) and drug-sensitive (3D7) strains of *P. falciparum,* as well as against HEK293 cells for preliminary cytotoxicity assessment. For comparison, we also re-examined the parent compound **1** alongside the current series as well as a number of reference compounds (Table 2). In addition to **1**, which demonstrated potent anti-parasitic activity (IC_{50} *Pf*-3D7 = 83.1 ± 16.1 nM, *Pf*-Dd2 = 81.7 ± 6.8 nM), three compounds from the series demonstrated potent inhibition of *Pf*-3D7 and *Pf*-Dd2 proliferation. The most active compounds included **6l**, **6n**, and **6q** which all inhibited parasitemia with IC_{50} values less than 100 nM, while other compounds examined demonstrated IC_{50} values between ~100-350 nM. Compound **6l** exhibited the most substantial improvement in anti-parasitic activity compared to the parent compound, showing IC_{50} values of 14.6 ± 0.8 nM against *Pf*-3D7 and 13.8 ± 0.5 nM against *Pf*-Dd2. Under our assay conditions, this activity is comparable to clinically used antimalarial drugs pyronaridine and chloroquine (IC_{50} *Pf*-3D7 = 7.0 ± 6.0 nM and 11.7 ± 3.5 nM, respectively), and approaching the range of the gold standard clinical treatments artesunate and dihydroartemisinin (IC_{50} *Pf*-3D7 = 1.6 ± 0.5 nM and 0.5 ± 0.1 nM respectively). Further, the compound series showed limited cytotoxicity against HEK293 with little inhibition of cellular proliferation at 10 μM. At 40 μM, we did observe inhibitory effects against HEK293, however, we were unable to calculate IC_{50} values as all compounds failed to reach a full inhibition plateau. Approximate selectivity indices were calculated for compounds that showed > 51 % inhibition at 40 μM and generally suggested excellent selectivity range (Table 2). The compound series therefore demonstrates substantial improvement in anti-malarial activity against cultured *P. falciparum* parasites and represents an exciting progression

of our anti-malarial compounds targeted against both the M1 and M17 aminopeptidases of *P. falciparum*.

Compound 6l does not inhibit MMPs. To investigate the potential for off-target effects of the compound series, we examined the ability of **6l**, the compound with the most potent cellular antiparasitic activity, to inhibit a panel of matrix metalloproteinases (MMPs). We assessed the activity of MMP2, 7, 8, 9, or 13 following inhibition with increasing concentrations of **6l** or control compounds (Marimastat or Tosedostat, Supplementary Table 4). As expected, the gelatinases (MMP2 and MMP9) were potently inhibited by Marimastat (IC_{50} = 0.43 and 3.1 nM respectively, Supplementary Table 4) and Tosedostat (IC_{50} = 0.19 and 1.5 μM respectively), whereas **6l** weakly inhibited MMP2 (IC_{50} = 17 μM) and did not inhibit MMP9 (IC_{50} > 1mM). Similar observations were made for collagenases (MMP8 and MMP13) as well as matrilysin (MMP7), which were all inhibited tightly by Marimastat and Tosedostat, but weakly, or not at all, by **6l**. Collectively, these findings show that **6l** shows almost no off-target inhibitory effects on MMPs. We additionally chose to examine the potential of **6l** to inhibit two human N-terminal aminopeptidases, aminopeptidase N (APN or CD13) and insulin-regulated aminopeptidase (IRAP). While **6l** showed only very weak inhibition of IRAP (no inhibition observed at **6l** concentrations less than 200 μM), it inhibits APN with reasonable affinity (K_i = 0.3 ± μM).

■ DISCUSSION

Antimalarial combination therapies have been the gold standard of malarial treatment since the ability of the *Plasmodium* parasite to generate resistance to drug monotherapies was understood. We have extended this strategy and used rational drug discovery to design compounds capable of potent dual inhibition of the *P. falciparum* M1 and M17 aminopeptidases, both key players of the essential hemoglobin digestion pathway. Based on the SAR of previously examined compound series', we generated novel hydroxamic-acid based compounds substituted with a range of hydrophobic moieties to probe the S1' subsites of *Pf*-M1 and *Pf*-M17. Further, we proposed that the

high identity of the M1 and M17 aminopeptidases between *Plasmodium* species would allow our compounds to act similarly against the *P. vivax* homologs. Herein, we have examined the ability of our compound series to inhibit the M1 and M17 aminopeptidases from both *P. falciparum* and *P. vivax*.

The compound series demonstrated substantial variability in the inhibition of *Pf*-M1 (nM to μM), which did not follow any clear and observable trend. By examination of the crystal structures of *Pf*-M1 bound to key compounds of the series, we determined this variation was due to different compound binding modes. Interestingly, the variation in inhibition potency was also observed for *Pv*-M1. However, while the overall trends were conserved, we found that the compounds inhibited *Pv*-M1 approximately 10-fold more potently than *Pf*-M1. This is despite high overall sequence conservation, and 100% identity in inhibitor-binding residues (based on the *Pf*-M1 crystal structures). The 10-fold change in inhibitor binding potencies are therefore likely to result from enzyme differences beyond the active site arrangement. Such differences could include the size/shape of the active site resulting from secondary/tertiary structure beyond the binding pocket. Alternatively, the difference may result from mechanistic features beyond active site chemistry, such as protein flexibility. Analysis of the M1 aminopeptidase superfamily has shown that conformational dynamics plays a critical role in substrate recognition and catalysis.[33, 34] It is therefore possible that differences in the enzyme conformational dynamics exist that cannot be predicted from the protein sequences, and that these dynamics play a role in inhibitor binding.

Similarly to M1 aminopeptidases, the inhibitor binding residues of the M17 homologs from *P. falciparum* and *P. vivax* are also highly conserved. This includes the binuclear metal binding site, which possess a highly conserved arrangement through the enzyme superfamily. The two metal sites bind divalent metal ions, most commonly Zn^{2+}, and have been characterized as 'regulatory' and 'catalytic' sites (site 1 and site 2, respectively). The 'catalytic' metal is coordinated by the side chains of conserved Lys, Asp, and Glu residues (Lys374, Asp379, and Glu461 in *Pf*-M17) and the 'regulatory' metal is coordinated by the sidechains of a conserved Asp and Glu (Asp379 and

Glu461 in *Pf*-M17) as well as the sidechain and mainchain oxygen of another Asp (Asp459 in *Pf*-M17). Occupation of the catalytic site is absolutely required for catalytic activity.[31] The observation that **6k** and **6i** are competing with the catalytic Zn^{2+} is therefore completely unexpected, and has substantial implications for drug discovery. By competing with both metal cofactor as well as substrate, the compound mechanism of inhibition has evolved, and competitive models of binding, that calculate inhibition constants on the basis of assay substrate concentration and affinity as well as inhibitor and enzyme concentration, may no longer be appropriate. Our strategy to target both the *Pv*-M17 as well as the *Pf*-M17 raises further questions about the ability of inhibitors to displace the metal cofactors. The trend in inhibitor binding potencies of *Pf*- versus *Pv*-M17 diverged as the compounds were substituted with bulky hydrophobic groups (**6l**–**6r** + **6k**, Figure 1B and Table 1). Differences in the ability of the compounds to displace the catalytic Zn^{2+} of the *Pf*- versus the *Pv*-M17 could account for the variation in compound binding trends. It is possible that differences in active site architecture and/or metal binding behavior between the *Pf*- and *Pv*-M17 enzymes exist which are not predicted by the close sequence similarity. In the wake of the observations for *Pf*-M17 reported here, the complete characterization of *Pv*-M17 metal binding behavior should be prioritized.

In some case, hydroxamate inhibitors developed as anticancer agents have suffered clinical failure. Discussions regarding the liabilities of the chemical class largely revolve around the potential for off-target activity against other zinc-dependent enzymes, which might lead to toxicity. However, the previous generations of hydroxamates were safely tested in thousands of humans for a variety of cancers.[35-37] The only toxicity noted was some muscle tenderness in the upper body girdle. This led to a very small number of patients limiting dosing, which resulted in ineffective treatment for those patients.[35-37] Otherwise the hydroxamate inhibitors (Marimastat and Batimastat) were considered safe for humans, demonstrating only minor off target activity at clinically used doses.[35-37] Irrespectively, given the reputation of hydroxamate inhibitors, we assessed the potential for the current series to cross-react. We examined the ability of **6l** to inhibit a panel of MMPs

(MMP2, 7, 8, 9, and 13), and additionally, two human N-terminal aminopeptidases (IRAP and APN). Compound **6l** exhibit very weak to no activity against the MMPs and IRAP, demonstrating low potential for off-target activity. However, inhibition of APN, the closest human homolog of the *Plasmodium* M1-aminopeptidases, was observed. APN is an anti-cancer therapeutic target, and it has clinically demonstrated that inhibition of APN activity does not result in any harmful side effects. [38] Therefore, while designing selectivity over APN should be considered in future optimization of this inhibitor series, we do not anticipate a high degree of selectivity over APN to be required for safe use of the compounds in humans.

Physiological activity of a multi-target inhibitor is difficult to predict from enzyme inhibition data, as the effect in live parasites may not be linearly correlated with inhibition of either/both targets.[39, 40] Throughout the development of the *Pf*-M1/*Pf*-M17 dual inhibitor compound series, we have observed a broad correlation of improved cellular potency with increasing either *Pf*-M1 or *Pf*-M17 inhibition potency.[15, 17, 20] Within the current series, we observed a substantial (> 5-fold) improvement in anti-plasmodial activity with compound **6l**. While exciting, the improvement is curious, in that it is does not directly reflect the *Pf*-M1 and *Pf*-M17 enzyme inhibition; **6l** is not the most potent dual inhibitor of the series, yet it clearly demonstrates the greatest potency of the series in the whole-cell *in vitro* assay. Compound **6l** is therefore a highly potent outlier. We propose three potential reasons for this deviation: (1) increasing the hydrophobicity of the compounds has a large effect on cellular penetration, (2) **6l** targets additional cellular processes, or (3) the conditions of the enzyme assays do not strictly reflect cellular conditions. Irrespectively, **6l** is a potent inhibitor of the four molecular targets examined herein, and demonstrates potent activity against cultured malaria parasites; it therefore represents a promising lead for further development of potent antimalarial therapeutics.

■ CONCLUSIONS

The rapid spread of drug resistant *Plasmodium* parasites is a major threat to global health. We have previously used a multi-target strategy to rationally design inhibitors capable of potent

inhibition of the *Pf*-M1 and *Pf*-M17 aminopeptidases, and validated their use in culture against both drug resistant and drug sensitive strains of the parasite. Herein we have expanded our strategy to target the M1 and M17 aminopeptidases from *P. vivax* with the aim to develop compounds capable of cross-species antimalarial activity. We designed a series of inhibitors that possess a novel chemical scaffold and mapped their structure-activity relationships against the four molecular targets *in vitro*. Excitingly, compounds possessing potent inhibitory activity against all four enzymes also demonstrated potent activity against cultured parasites, and showed no observable toxicity against human cells. This novel series of hydroxamic acid compounds therefore represents an exciting lead in the design of novel antimalarial therapeutics. They operate via a novel, known mechanism of action, and further, have the potential to be clinically effective against multiple *Plasmodium* species.

■ EXPERIMENTAL SECTION

Chemistry. Synthetic Materials and Methods. Chemicals and solvents were purchased from standard suppliers and used without further purification. ^{1}H NMR, ^{13}C NMR and ^{19}F NMR spectra were recorded on a Bruker Avance Nanobay III 400MHz Ultrashield Plus spectrometer at 400.13 MHz, 100.61 MHz, and 376.50 MHz, respectively. Chemical shifts (δ) are recorded in parts per million (ppm) with reference to the chemical shift of the deuterated solvent. Unless otherwise stated, samples were dissolved in $CDCl_3$. Coupling constants (*J*) and carbon-fluorine coupling constants (J_{CF}) are recorded in Hz and multiplicities are described by singlet (s), doublet (d), triplet (t), quadruplet (q), broad (br), multiplet (m), doublet of doublets (dd), doublet of triplets (dt). Overlapped non-equivalent ^{13}C peaks were identified by HSQC and HMBC experiments and are indicated with (2C) after the identified overlapped signal. LC-MS was performed using either system A or B. System A: an Agilent 6100 Series Single Quad coupled to an Agilent 1200 Series HPLC using a Phenomenex Luna C8 (2) 50 x 4.6 mm, 5 micron column. The following buffers were used; buffer A: 0.1% formic acid in H_2O; buffer B: 0.1% formic acid in MeCN. Samples were run at a flow rate of 0.5 mL/min for 10 min: 0–4 min 5–100% buffer B in buffer A, 4–7 min 100% buffer B, 7–9 min 100–5% buffer B in buffer A, 9–10 min 5% buffer B in buffer A. Mass spectra were acquired in positive and negative ion mode with a scan range of 100–1000 *m/z*. UV detection was carried out at 254 nm. System B: an Agilent 6120 Series Single Quad coupled to an Agilent 1260 Series HPLC using a Poroshell 120 EC-C18 50 x 3.0 mm, 2.7 micron column. The following buffers were used; buffer A: 0.1% formic acid in H_2O; buffer B: 0.1% formic acid in MeCN. Samples were run at a flow rate of 0.5 mL/min for 5 min; 0–1 min 5% buffer B in buffer A, 1–2.5 min 5–100% buffer B in buffer A, 2.5–3.8 min 100% buffer B, 3.8–4 min 100–5% buffer B in buffer A, 4–5 min 5% buffer B in buffer A. Mass spectra were acquired in positive and negative ion mode with a scan range of 100–1000 *m/z*. UV detection was carried out at 214 and 254 nm.

Preparative HPLC was performed using an Agilent 1260 infinity coupled with a binary preparative pump and Agilent 1260 FC-PS fraction collector, using Agilent OpenLAB CDS

software (Rev C.01.04), and an Altima C8 22 x 250 mm 5 micron column. The following buffers were used; buffer A: 0.1% TFA in H_2O; buffer B: 0.1% TFA in MeCN, with sample being run at a gradient of 5–100% buffer B in buffer A over 20 min, at a flow rate of 20 mL/min. All screening compounds were of >95% purity unless specified in the individual monologue.

General Procedure A: Formation of amide bond using acid chlorides. The amine (1.0 eq) was dissolved in CH_2Cl_2 (10 mL/mmol of amine). The flask was evacuated and flushed with nitrogen. Et_3N (2.2 eq) was added followed by the acid chloride (1.1 eq). The reaction mixture was stirred at rt for 2 h. Water was added and the aqueous layer further extracted with CH_2Cl_2 (3 times). The combined organic layers were dried over Na_2SO_4, filtered and concentrated under reduced pressure. The crude product was purified by FCC.

General Procedure B: Formation of amide bond using HCTU. The acid (1.05 eq) and HCTU (1.1 eq) were stirred in DMF (1 mL/mmol of amine). *N,N*-diisopropylethylamine (2.2 eq) was added followed by a solution of the amine (1.0 eq) in CH_2Cl_2 (1 mL/mmol of amine). The reaction mixture was stirred at room temperature for 2 h. Half saturated $NaHCO_3$ (aq) was added and the mixture extracted with Et_2O (3 times). The combined organic layers were dried over Na_2SO_4, filtered and concentrated under reduced pressure. The crude product was purified by FCC.

General Procedure C: Formation of amide bond using EDCI. A mixture of amine (1.0 eq), acid (1.2 eq), EDCI (1.2 eq) and DMAP (1.3 eq) in CH_2Cl_2 (10 mL/mmol of amine) was stirred at rt under N_2 overnight. The mixture was diluted with CH_2Cl_2, washed with 2M HCl (aq), saturated $NaHCO_3$ (aq), then brine. The organic layer was dried over Na_2SO_4, filtered and concentrated under reduced pressure. The crude product was purified by FCC.

General Procedure D: Aminolysis of methyl ester to hydroxamic acid. The appropriate methyl ester (1.0 eq) was dissolved in anhydrous MeOH (5 mL/mmol of ester) at rt. $NH_2OH.HCl$ (4.0 eq) was added followed by KOH (5M in anhydrous MeOH, 5.0 eq). The mixture was stirred at rt overnight and monitored by LC-MS analysis. The mixtures were directly dry-loaded on to Isolute HM-N® (Biotage), before purification by FCC (eluent MeOH/ CH_2Cl_2 0:100 to 10:90).

Methyl 2-amino-2-(4-bromophenyl)acetate (3). To a mixture of 2-amino-2-(4-bromophenyl)acetic acid (2.0 g, 8.7 mmol) in MeOH (87 mL) was added concentrated H_2SO_4 (0.8 mL, 15.7 mmol) dropwise. The reaction mixture was refluxed for 30 h. The solvent was concentrated *in vacuo* and the resulting residue was basified with saturated $NaHCO_3$ (50 mL), then extracted with CH_2Cl_2 (3 x 50 mL). The combined organic layers were dried over Na_2SO_4, filtered and concentrated under reduced pressure to give the title compound as a yellow oil (2.0 g, 94%). ^{1}H NMR δ 7.51–7.45 (m, 2H), 7.30–7.24 (m, 2H), 4.59 (s, 1H), 3.70 (s, 3H), 1.85 (s, 2H); ^{13}C NMR δ 174.1, 139.3, 132.0, 128.7, 122.2, 58.3, 52.7; *m/z* MS (TOF ES$^+$) $C_9H_{11}BrNO_2$ $[MH]^+$ calcd 244.0, found 244.1; LC-MS t_R = 3.2 min.

Methyl 2-amino-2-(3',4',5'-trifluoro-[1,1'-biphenyl]-4-yl)acetate (4). Compound **3** (2.0 g, 8.2 mmol) and 3,4,5-trifluorophenylboronic acid (2.2 g, 12.3 mmol) were dispersed in degassed THF (30 mL) and degassed 1M $Na_2CO_{3\ (aq)}$ (10 mL). A steady stream of N_2 was bubbled through the mixture for 5 min, before adding $PdCl_2(PPh_3)_2$ (0.58 g, 0.82 mmol). The mixture was refluxed for 2 h, then the THF was concentrated *in vacuo*. The mixture was diluted with EtOAc (50 mL) and water (50 mL), and the aqueous layer extracted further with EtOAc (2 x 50 mL). The combined organic layers were dried over Na_2SO_4, filtered and concentrated. The crude product was purified by FCC (MeOH/CH_2Cl_2 0:100 to 10:90) to give the title compound as a beige foam (1.6 g, 65%). ^{1}H NMR (DMSO-d_6) δ 9.04 (br. s, 2H), 7.85 (d, J = 8.1 Hz, 2H), 7.82–7.68 (m, 2H), 7.61 (d, J = 8.2 Hz, 2H), 5.40 (s, 1H), 3.74 (s, 3H); ^{19}F NMR (DMSO-d_6) δ -134.70 (d, J = 21.7 Hz), -162.73 (dd, J = 21.7/21.7 Hz); ^{13}C NMR (DMSO-d_6) δ 168.9, 150.7 (ddd, J_{CF} = 246.6/9.8/4.1 Hz), 138.6 (dt, J_{CF} = 250.4/15.8 Hz), 138.0, 135.9 (td, J_{CF} = 8.1/4.5 Hz), 132.9, 128.9, 127.5, 111.8–111.2 (m), 55.0, 53.3; *m/z* MS (TOF ES$^+$) $C_{15}H_{13}F_3NO_2$ $[MH]^+$ calcd 296.1, found 296.1; LC-MS t_R = 3.0 min.

Methyl 2-isobutyramido-2-(3',4',5'-trifluoro-[1,1'-biphenyl]-4-yl)acetate (5a). Compound **4** (200 mg, 0.68 mmol) was converted to the title compound according to General Procedure A using isobutyryl chloride (78 µL, 0.75 mmol), to give 141 mg (57%) of white solid. ^{1}H NMR δ 7.54–7.38 (m, 4H), 7.21–7.09 (m, 2H), 6.58 (d, J = 6.5 Hz, 1H), 5.61 (d, J = 6.9 Hz, 1H), 3.75 (s,

3H), 2.58–2.36 (m, 1H), 1.19 (d, J = 6.9 Hz, 3H), 1.16 (d, J = 6.9 Hz, 3H); ^{19}F NMR δ -133.91 (d, J = 20.6 Hz), -162.19 (dd, J = 20.7/20.7 Hz); ^{13}C NMR δ 176.4, 171.4, 151.5 (ddd, J_{CF} = 249.7/10.1/4.2 Hz), 141.0–137.9 (m, 2C), 137.2, 136.7 (td, J_{CF} = 7.7/4.5 Hz), 128.0, 127.5, 111.4–110.8 (m), 55.9, 53.0, 35.3, 19.5, 19.4; *m/z* MS (TOF ES$^+$) $C_{19}H_{19}F_3NO_3$ [MH]$^+$ calcd 366.1, found 365.9; LC-MS t_R = 3.5 min.

Methyl 2-propionamido-2-(3',4',5'-trifluoro-[1,1'-biphenyl]-4-yl)acetate (5b). Compound **4** (200 mg, 0.68 mmol) was converted to the title compound according to General Procedure A using propionyl chloride (65 μL, 0.75 mmol), to give 205 mg (86%) of pale yellow solid. ^{1}H NMR δ 7.51–7.43 (m, 4H), 7.21–7.09 (m, 2H), 6.54 (d, J = 6.7 Hz, 1H), 5.63 (d, J = 7.0 Hz, 1H), 3.76 (s, 3H), 2.30 (qd, J = 7.6/3.2 Hz, 2H), 1.17 (t, J = 7.6 Hz, 3H); ^{19}F NMR δ -133.88 (d, J = 20.4 Hz), -162.14 (dd, J = 20.6/20.6 Hz); ^{13}C NMR δ 173.2, 171.4, 151.5 (ddd, J_{CF} = 249.7/10.1/4.3 Hz), 139.4 (dt, J_{CF} = 34.1/15.3 Hz), 138.4, 137.2, 136.6 (td, J_{CF} = 7.8/4.7 Hz), 128.1, 127.5, 111.5–110.8 (m), 56.0, 53.0, 29.4, 9.6; *m/z* MS (TOF ES$^+$) $C_{18}H_{17}F_3NO_3$ [MH]$^+$ calcd 352.1, found 351.9; LC-MS t_R = 3.4 min.

Methyl 2-(3',4',5'-trifluoro-[1,1'-biphenyl]-4-yl)-2-(3,3,3-trifluoropropanamido)acetate (5c). Compound **4** (200 mg, 0.68 mmol) was converted to the title compound according to General Procedure B using trifluoromethylacetic acid (63 μL, 0.71 mmol), to give 140 mg (51%) of white solid. ^{1}H NMR δ 7.46 (dd, J = 22.6/8.1 Hz, 4H), 7.23–7.09 (m, 2H), 7.00 (d, J = 6.0 Hz, 1H), 5.62 (d, J = 6.6 Hz, 1H), 3.77 (s, 3H), 3.15 (q, J = 10.5 Hz, 2H); ^{19}F NMR δ -62.85, -133.79 (d, J = 20.5 Hz), -161.95 (dd, J = 20.6/20.6 Hz); ^{13}C NMR δ 170.8, 162.1 (app. d, J_{CF} = 3.4 Hz), 151.6 (ddd, J_{CF} = 250.1/9.9/4.3 Hz), 139.60 (dt, J_{CF} = 251.5/14.8 Hz), 138.9, 136.8–136.3 (m), 136.2, 128.0, 127.7, 123.9 (app. d, J_{CF} = 276.8 Hz), 111.5–110.9 (m), 56.5, 53.4, 41.6 (q, J_{CF} = 29.8 Hz); *m/z* MS (TOF ES$^+$) $C_{18}H_{14}F_6NO_3$ [MH]$^+$ calcd 406.1, found 406.1; LC-MS t_R = 3.8 min.

Methyl 2-(2,3,3,3-tetrafluoropropanamido)-2-(3',4',5'-trifluoro-[1,1'-biphenyl]-4-yl)acetate (5d). Compound **4** (150 mg, 0.51 mmol) was converted to the title compound according to General Procedure C using 2,3,3,3-tetrafluoropropanoic acid (59 μL, 0.61 mmol), to give 110 mg

(51%, mixture of diastereomers) of white solid. ^{1}H NMR δ 7.56–7.41 (m, 5H), 7.22–7.11 (m, 2H), 5.64 (d, *J* = 6.8 Hz, 1H), 5.23–4.98 (m, 1H), 3.80 (s, 3H); ^{19}F NMR δ -75.86 (dd, *J* = 33.7/11.2 Hz), -133.74 (dd, *J* = 36.3/20.5 Hz), -161.85 (dt, *J* = 41.1/20.5 Hz), -202.47 – -202.75 (m); *m/z* MS (TOF ES$^-$) $C_{18}H_{11}F_7NO_3$ [M]$^-$ calcd 422.1, found 422.0; LC-MS t_R = 3.5 min.

Methyl 2-(2,2,3,3,3-pentafluoropropanamido)-2-(3',4',5'-trifluoro-[1,1'-biphenyl]-4-yl)acetate (5e). Compound **4** (150 mg, 0.51 mmol) was converted to the title compound according to General Procedure C using 2,2,3,3,3-pentafluoropropanoic acid (64 μL, 0.61 mmol), to give 15 mg (7%) of white solid. ^{1}H NMR δ 7.58 (d, *J* = 6.1 Hz, 1H), 7.54–7.41 (m, 4H), 7.22–7.12 (m, 2H), 5.59 (d, *J* = 6.7 Hz, 1H), 3.81 (s, 3H); ^{19}F NMR δ -82.71–- 82.74 (m), -122.91–-122.96 (m), -133.68 (d, *J* = 20.5 Hz), -161.72 (dd, *J* = 20.5/20.5 Hz); ^{13}C NMR δ 169.8, 157.1, 151.6 (ddd, *J* = 250.1/10.0/4.3 Hz), 139.7 (dt, *J* = 252.6/15.3 Hz), 139.4–139.2 (m), 136.7–136.1 (m), 135.0, 128.0, 127.9, 117.9 (dt, *J* = 285.6/33.8 Hz), 111.6–111.1 (m), 107.9–106.1 (m), 56.5, 53.7.*m/z* MS (TOF ES$^-$) $C_{18}H_{10}F_8NO_3$ [M]$^-$ calcd 440.1, found 440.1; LC-MS t_R = 3.5 min.

Methyl 2-(cyclopropanecarboxamido)-2-(3',4',5'-trifluoro-[1,1'-biphenyl]-4-yl)acetate (5f). Compound **4** (140 mg, 0.47 mmol) was converted to the title compound according to General Procedure A using cyclopropanecarbonyl chloride (47 μL, 0.52 mmol), to give 150 mg (87%) of white solid. ^{1}H NMR δ 7.52–7.43 (m, 4H), 7.20–7.10 (m, 2H), 6.75 (br. d, *J* = 6.8 Hz, 1H), 5.65 (d, *J* = 6.9 Hz, 1H), 3.76 (s, 3H), 1.52–1.44 (m, 1H), 1.04–0.92 (m, 2H), 0.86–0.70 (m, 2H); ^{19}F NMR δ -133.89 (d, *J* = 20.5 Hz), -162.18 (dd, *J* = 20.5/20.5 Hz); ^{13}C NMR δ 173.2, 171.4, 151.4 (ddd, J_{CF} = 249.7/10.0/4.2 Hz), 141.1–137.8 (m), 138.2, 137.2, 136.6 (td, J_{CF} = 7.8/4.6 Hz), 128.0, 127.4, 111.2–110.8 (m), 56.2, 52.9, 14.5, 7.60, 7.56; *m/z* MS (TOF ES$^+$) $C_{19}H_{17}F_3NO_3$ [MH]$^+$ calcd 364.1, found 363.9; LC-MS t_R = 3.5 min.

Methyl 2-(cyclobutanecarboxamido)-2-(3',4',5'-trifluoro-[1,1'-biphenyl]-4-yl)acetate (5g). Compound **3** (160 mg, 0.66 mmol) was converted to methyl 2-(4-bromophenyl)-2-(cyclobutanecarboxamido)acetate according to General Procedure A using cyclobutanecarbonyl chloride (82 μL, 0.72 mmol). The crude product was reacted with 3,4,5-trifluorophenylboronic acid

(138 mg, 0.79 mmol), $Pd(PPh_3)_2Cl_2$ (14 mg, 0.02 mmol), Na_2CO_3 (1M, 1.3 mL) in THF (3.9 mL) in a sealed microwave vial and heated at 100 °C for 2 h. After cooling, the mixture was diluted with EtOAc (10 mL) and water (10 mL), and the mixture extracted with EtOAc. The organic layer was dried over Na_2SO_4, filtered and concentrated. The crude product was purified by FCC to give 220 mg (89%) of a colourless oil. ^{1}H NMR δ 7.51–7.40 (m, 4H), 7.21–7.10 (m, 2H), 6.46 (br. d, *J* = 6.8 Hz, 1H), 5.61 (d, *J* = 6.9 Hz, 1H), 3.76 (s, 3H), 3.10 (pd, *J* = 8.5/0.9 Hz, 1H), 2.37–2.12 (m, 4H), 2.03–1.83 (m, 2H); ^{19}F NMR δ -133.87 (d, *J* = 20.6 Hz), -162.12 (dd, *J* = 20.6/20.6 Hz); ^{13}C NMR δ 175.2, 171.3, 151.5 (ddd, *J* = 249.7/10.0/4.2 Hz), 139.4 (dt, *J* = 252.2/15.4 Hz), 138.4, 136.9, 136.7–136.4 (m), 128.0, 127.4, 111.5–110.6 (m), 56.1, 53.0, 39.6, 25.26, 25.25, 18.2; *m/z* MS (TOF ES$^+$) $C_{20}H_{19}F_3NO_3$ $[MH]^+$ calcd 378.1, found 377.9; LC-MS t_R = 3.5 min.

Methyl 2-(cyclopentanecarboxamido)-2-(3',4',5'-trifluoro-[1,1'-biphenyl]-4-yl)acetate (5h). Compound **4** (130 mg, 0.44 mmol) was converted to the title compound according to General Procedure A using cyclopentanecarbonyl chloride (60 µL, 0.48 mmol), to give 70 mg (41%) of yellow foamy solid. ^{1}H NMR δ 7.51–7.37 (m, 4H), 7.19–7.08 (m, 2H), 6.66 (d, *J* = 6.9 Hz, 1H), 5.62 (d, *J* = 7.0 Hz, 1H), 3.74 (s, 3H), 2.70–2.59 (m, 1H), 1.95–1.49 (m, 8H); ^{19}F NMR δ -133.9 (d, *J* = 20.5 Hz), -162.2 (dd, *J* = 20.5/20.5 Hz); ^{13}C NMR δ 175.9, 171.5, 151.5 (ddd, J_{CF} = 249.8/10.0/4.2 Hz), 139.5 (dt, J_{CF} = 252.0/15.4 Hz), 138.4–138.3 (m), 137.2, 136.7 (td, J_{CF} = 7.8/4.6 Hz), 128.0, 127.5, 111.6–110.9 (m), 56.1, 53.1, 45.5, 30.4, 30.3, 26.0 (2C); *m/z* MS (TOF ES$^+$) $C_{21}H_{21}F_3NO_3$ $[MH]^+$ calcd 392.1, found 392.1; LC-MS t_R = 6.8 min.

Methyl 2-(cyclohexanecarboxamido)-2-(3',4',5'-trifluoro-[1,1'-biphenyl]-4-yl)acetate (5i). Compound **4** (130 mg, 0.44 mmol) was converted to the title compound according to General Procedure A using cyclohexanecarbonyl chloride (64 µL, 0.48 mmol), to give 50 mg (28%) of pale yellow solid. ^{1}H NMR δ 7.51–7.37 (m, 4H), 7.21–7.07 (m, 2H), 6.59 (d, *J* = 6.9 Hz, 1H), 5.61 (d, *J* = 7.0 Hz, 1H), 3.75 (s, 3H), 2.19 (tt, *J* = 11.7/3.5 Hz, 1H), 1.96–1.62 (m, 5H), 1.53–1.13 (m, 5H); ^{19}F NMR δ -133.9 (d, *J* = 20.5 Hz), -162.2 (dd, *J* = 20.6/20.6 Hz); ^{13}C NMR δ 175.5, 171.5, 151.5 (ddd, J_{CF} = 249.8/10.0/4.3 Hz), 139.5 (dt, J_{CF} = 252.2/15.4 Hz), 138.5–138.4 (m), 137.3, 136.7 (td,

J_{CF} = 7.9/4.8 Hz), 128.0, 127.5, 111.5–110.8 (m), 55.9, 53.1, 45.2, 29.7, 29.5, 25.79, 25.75, 25.7; *m/z* MS (TOF ES$^+$) $C_{22}H_{23}F_3NO_3$ [MH]$^+$ calcd 406.2, found 406.2; LC-MS t_R = 4.0 min.

Methyl 2-(tetrahydro-2H-pyran-4-carboxamido)-2-(3',4',5'-trifluoro-[1,1'-biphenyl]-4-yl)acetate (5j). Compound **4** (120 mg, 0.41 mmol) was converted to the title compound according to General Procedure B using tetrahydropyrancarboxylic acid (56 mg, 0.43 mmol), to give 126 mg (76%) of white solid. ^{1}H NMR δ 7.50–7.40 (m, 4H), 7.20–7.09 (m, 2H), 6.64 (d, *J* = 6.8 Hz, 1H), 5.60 (d, *J* = 6.8 Hz, 1H), 4.08–3.96 (m, 2H), 3.76 (s, 3H), 3.47–3.37 (m, 2H), 2.51–2.40 (m, 1H), 1.88–1.73 (m, 4H); ^{19}F NMR δ -133.8 (d, *J* = 20.5 Hz), -162.0 (dd, *J* = 20.5/20.5 Hz); ^{13}C NMR δ 174.0, 171.3, 151.6 (ddd, J_{CF} = 250.0/10.1/4.3 Hz), 139.6 (dt, J_{CF} = 252.3/15.2 Hz), 138.7, 136.9, 136.7–136.4 (m), 128.0, 127.7, 111.5–110.9 (m), 67.3, 56.1, 53.3, 42.0, 38.8, 29.2, 29.1; *m/z* MS (TOF ES$^+$) $C_{21}H_{21}F_3NO_4$ [MH]$^+$ calcd 408.1, found 408.2; LC-MS t_R = 3.7 min.

Methyl 2-((3r,5r,7r)-adamantane-1-carboxamido)-2-(3',4',5'-trifluoro-[1,1'-biphenyl]-4-yl)acetate (5k). Compound **4** (200 mg, 0.68 mmol) was converted to the title compound according to General Procedure A using 1-adamantanecarbonyl chloride (148 mg, 0.75 mmol), to give 150 mg (48%) of white solid. ^{1}H NMR δ 7.50–7.40 (m, 4H), 7.21–7.09 (m, 2H), 6.77 (d, *J* = 6.6 Hz, 1H), 5.57 (d, *J* = 6.6 Hz, 1H), 3.75 (s, 3H), 2.10–2.02 (m, 3H), 1.89 (d, *J* = 2.7 Hz, 6H), 1.80–1.65 (m, 6H); ^{19}F NMR δ -133.9 (d, *J* = 20.6 Hz), -162.2 (dd, *J* = 20.6/20.6 Hz); ^{13}C NMR δ 177.7, 171.5, 151.6 (ddd, J_{CF} = 249.7/10.0/4.3 Hz), 139.5 (dt, J_{CF} = 252.2/15.4 Hz), 138.5–138.4 (m), 137.2, 136.7 (td, J_{CF} = 7.7/4.4 Hz), 127.9, 127.6, 111.4–110.9 (m), 56.0, 53.1, 39.2, 36.5, 28.1; LC-MS R_t = 4.4 min (compound did not ionize).

Methyl 2-(3,3-dimethylbutanamido)-2-(3',4',5'-trifluoro-[1,1'-biphenyl]-4-yl)acetate (5l). Compound **4** (149 mg, 0.50 mmol) was converted to the title compound according to General Procedure A using 3,3-dimethylbutyryl chloride (77 μL, 0.56 mmol), to give 110 mg (55%) of white solid. ^{1}H NMR δ 7.50–7.41 (m, 4H), 7.20–7.10 (m, 2H), 6.47 (d, *J* = 6.7 Hz, 1H), 5.62 (d, *J* = 6.9 Hz, 1H), 3.75 (s, 3H), 2.13 (s, 2H), 1.03 (s, 9H); ^{19}F NMR δ -133.9 (d, *J* = 20.6 Hz), -162.2 (dd, *J* = 20.6/20.6 Hz); ^{13}C NMR δ 171.4, 171.2, 151.6 (ddd, J_{CF} = 249.8/10.0/4.3 Hz), 139.5 (dt, J_{CF} =

252.3/15.3 Hz), 138.66–138.33 (m), 137.2, 137.0–136.0 (m), 128.2, 127.5, 111.4–111.0 (m), 56.1, 53.1, 50.3, 31.2, 29.9; *m/z* MS (TOF ES$^+$) $C_{21}H_{23}F_3NO_3$ [MH]$^+$ calcd 394.2, found 394.2; LC-MS t_R = 4.0 min.

Methyl 2-(2-cyclopropylacetamido)-2-(3',4',5'-trifluoro-[1,1'-biphenyl]-4-yl)acetate (5m). Compound **4** (200 mg, 0.68 mmol) was converted to the title compound according to General Procedure B using cyclopropylacetic acid (70 µL, 0.71 mmol), to give 141 mg (55%) of white solid. ^{1}H NMR δ 7.50–7.42 (m, 4H), 7.19–7.08 (m, 3H), 5.64 (d, *J* = 7.0 Hz, 1H), 3.75 (s, 3H), 2.28–2.14 (m, 2H), 1.08–0.95 (m, 1H), 0.68–0.60 (m, 2H), 0.28–0.18 (m, 2H); ^{19}F NMR δ -133.9 (d, *J* = 20.5 Hz), -162.2 (dd, *J* = 20.5/20.5 Hz); ^{13}C NMR δ 172.1, 171.3, 151.5 (ddd, J_{CF} = 249.8/10.0/4.2 Hz), 139.5 (dt, J_{CF} = 252.1/15.3 Hz), 138.5–138.4 (m), 137.1, 136.6 (td, J_{CF} = 7.8/4.7 Hz), 128.0, 127.5, 111.6–110.8 (m), 56.0, 53.1, 41.2, 7.1, 4.71, 4.68; *m/z* MS (TOF ES$^+$) $C_{20}H_{19}F_3NO_3$ [MH]$^+$ calcd 378.1, found 378.1; LC-MS t_R = 3.8 min.

Methyl 2-(2-cyclobutylacetamido)-2-(3',4',5'-trifluoro-[1,1'-biphenyl]-4-yl)acetate (5n). Compound **4** (200 mg, 0.68 mmol) was converted to the title compound according to General Procedure B using cyclobutylacetic acid (74 µL, 0.71 mmol), to give 160 mg (60%) of white solid. ^{1}H NMR δ 7.49–7.38 (m, 4H), 7.17–7.09 (m, 2H), 6.73 (d, *J* = 6.9 Hz, 1H), 5.60 (d, *J* = 6.9 Hz, 1H), 3.74 (s, 3H), 2.78–2.59 (m, 1H), 2.38 (d, *J* = 7.7 Hz, 2H), 2.20–2.05 (m, 2H), 1.96–1.65 (m, 4H); ^{19}F NMR δ -133.9 (d, *J* = 20.5 Hz), -162.2 (dd, *J* = 20.6/20.6 Hz); ^{13}C NMR δ 172.0, 171.3, 151.5 (ddd, J_{CF} = 249.8/10.0/4.3 Hz), 139.5 (dt, J_{CF} = 252.2/15.4 Hz), 138.4 (d, J_{CF} = 1.6 Hz), 137.0, 136.6 (td, J_{CF} = 7.8/4.6 Hz), 128.0, 127.5, 111.3–110.9 (m), 56.0, 53.1, 43.4, 32.7, 28.42, 28.40, 18.6; *m/z* MS (TOF ES$^+$) $C_{21}H_{21}F_3NO_3$ [MH]$^+$ calcd 392.1, found 392.1; LC-MS t_R = 3.9 min.

Methyl 2-(2-cyclopentylacetamido)-2-(3',4',5'-trifluoro-[1,1'-biphenyl]-4-yl)acetate (5o). Compound **4** (120 mg, 0.41 mmol) was converted to the title compound according to General Procedure B using cyclopentylacetic acid (54 µL, 0.43 mmol), to give 140 mg (85%) of white solid. ^{1}H NMR δ 7.51–7.40 (m, 4H), 7.20–7.10 (m, 2H), 6.59 (d, *J* = 6.9 Hz, 1H), 5.63 (d, *J* = 6.9 Hz,

1H), 3.75 (s, 3H), 2.33–2.16 (m, 3H), 1.90–1.46 (m, 6H), 1.24–1.05 (m, 2H); ^{19}F NMR δ -133.9 (d, J = 20.5 Hz), -162.2 (dd, J = 20.6/20.6 Hz); ^{13}C NMR δ 172.4, 171.4, 151.6 (ddd, J_{CF} = 249.8/10.1/4.4 Hz), 139.5 (dt, J_{CF} = 252.2/15.5 Hz), 138.5–138.4 (m), 137.2, 136.7–136.6 (m), 128.1, 127.5, 111.5–110.9 (m), 56.1, 53.1, 42.8, 37.2, 32.68, 32.65, 25.09, 25.08; *m/z* MS (TOF ES$^+$) $C_{22}H_{23}F_3NO_3$ [MH]$^+$ calcd 406.2; found 406.2; LC-MS t_R: 4.0 min.

Methyl 2-(2-cyclohexylacetamido)-2-(3',4',5'-trifluoro-[1,1'-biphenyl]-4-yl)acetate (5p). Compound **4** (120 mg, 0.41 mmol) was converted to the title compound according to General Procedure B using cyclohexylacetic acid (61 mg, 0.43 mmol), to give 97 mg (57%) of white solid. ^{1}H NMR δ 7.50–7.41 (m, 4H), 7.20–7.10 (m, 2H), 6.52 (d, J = 6.8 Hz, 1H), 5.63 (d, J = 6.9 Hz, 1H), 3.75 (s, 3H), 2.18–2.07 (m, 2H), 1.86–1.57 (m, 6H), 1.34–0.85 (m, 5H); ^{19}F NMR δ -133.9 (d, J = 20.5 Hz), -162.2 (dd, J = 20.5/20.5 Hz); ^{13}C NMR δ 172.0, 171.4, 151.6 (ddd, J_{CF} = 249.8/9.9/4.2 Hz), 139.5 (dt, J_{CF} = 254.8/15.3 Hz), 138.6–138.4 (m), 137.2, 136.8–136.4 (m), 128.1, 127.6, 111.5–111.0 (m), 56.1, 53.1, 44.6, 35.5, 33.3, 33.2, 26.3, 26.2 (2C); *m/z* MS (TOF ES$^+$) $C_{23}H_{25}F_3NO_3$ [MH]$^+$ calcd 420.2; found 420.3; LC-MS t_R: 4.1 min.

Methyl 2-(2-(cuban-1-yl)acetamido)-2-(3',4',5'-trifluoro-[1,1'-biphenyl]-4-yl)acetate (5q). Compound **4** (270 mg, 0.91 mmol) was converted to the title compound according to General Procedure B using 2-((2*r*,3*r*,5*r*,6*r*,7*r*,8*r*)-cuban-1-yl)acetic acid (156 mg, 0.96 mmol), to give 261 mg (65%) of white solid. ^{1}H NMR δ 7.49–7.38 (m, 4H), 7.18–7.07 (m, 2H), 6.77 (d, J = 7.0 Hz, 1H), 5.62 (d, J = 7.0 Hz, 1H), 3.94–3.80 (m, 7H), 3.71 (s, 3H), 2.66–2.48 (m, 2H); ^{19}F NMR δ -133.9 (d, J = 20.5 Hz), -162.3 (dd, J = 20.5/20.5 Hz); ^{13}C NMR δ 171.1, 170.2, 151.4 (ddd, J_{CF} = 249.7/10.0/4.2 Hz), 139.3 (dt, J_{CF} = 26.7/15.4 Hz), 138.3–138.1 (m), 137.2, 136.6 (td, J_{CF} = 7.7/4.6 Hz), 127.9, 127.3, 111.3–110.4 (m), 55.8, 55.0, 52.9, 49.0, 48.3, 44.2, 40.3; *m/z* MS (TOF ES$^+$) $C_{25}H_{21}F_3NO_3$ [MH]$^+$ calcd 440.1; found 440.2; LC-MS t_R: 3.6 min.

Methyl 2-(2-(bicyclo[2.2.1]heptan-2-yl)acetamido)-2-(3',4',5'-trifluoro-[1,1'-biphenyl]-4-yl)acetate (5r). Compound **4** (200 mg, 0.68 mmol) was converted to the title compound according to General Procedure B using 2-norbornaneacetic acid (104 μL, 0.71 mmol), to give 170 mg (58%)

of white solid. ^{1}H NMR δ 7.50–7.39 (m, 4H), 7.19–7.07 (m, 2H), 6.91–6.77 (m, 1H), 5.68–5.57 (m, 1H), 3.75 (d, J = 0.8 Hz, 3H), 2.29–2.17 (m, 2H), 2.15–2.04 (m, 1H), 2.01–1.82 (m, 2H), 1.56–1.36 (m, 3H), 1.32–0.99 (m, 5H); ^{19}F NMR δ -133.9 (dd, J = 20.4/0.8 Hz), -162.1 (td, J = 20.5/2.6 Hz); ^{13}C NMR δ 172.7, 171.2, 151.5 (ddd, J_{CF} = 249.9/10.0/4.3 Hz), 139.5 (dt, J_{CF} = 252.2/15.4 Hz), 138.5, 136.8, 136.7–136.2 (m), 128.01, 128.00,* 127.48, 127.46,* 111.3–110.8 (m), 56.2, 53.1, 43.30, 43.25,* 41.21, 41.19,* 39.0, 38.9,* 37.80, 37.78,* 36.83, 36.82,* 35.32, 35.30,* 29.83, 29.80,* 28.6, 28.5* [NB: All signals with an *correspond to the 2nd rotamer (50:50)]; *m/z* MS (TOF ES^{+}) $C_{24}H_{25}F_3NO_3$ [MH]$^{+}$ calcd 432.2; found 432.2; LC-MS t_R: 4.1 min.

***N*-(2-(Hydroxyamino)-2-oxo-1-(3',4',5'-trifluoro-[1,1'-biphenyl]-4-yl)ethyl)isobutyramide (6a).** Compound **5a** (141 mg, 0.39 mmol) was converted to the corresponding hydroxamic acid according to General Procedure D to give 130 mg (92%) of an oily white solid. ^{1}H NMR (DMSO-d_6) δ 11.02 (s, 1H), 9.03 (s, 1H), 8.57 (d, J = 8.5 Hz, 1H), 7.76–7.63 (m, 4H), 7.50 (d, J = 8.3 Hz, 2H), 5.42 (d, J = 8.5 Hz, 1H), 2.74–2.56 (m, 1H), 1.00 (d, J = 6.8 Hz, 3H), 0.97 (d, J = 6.8 Hz, 3H); ^{19}F NMR (DMSO-d_6) δ -134.93 (d, J = 21.7 Hz), -163.54 (dd, J = 21.7/21.7 Hz); ^{13}C NMR (DMSO-d_6) δ 176.1, 166.7, 150.7 (ddd, J_{CF} = 246.7/9.7/4.2 Hz), 139.5, 139.9–136.9 (m), 136.8–136.5 (m), 136.2, 127.6, 126.8, 111.5–110.9 (m), 53.3, 33.4, 19.6, 19.5; *m/z* HRMS (TOF ES^{+}) $C_{18}H_{18}F_3N_2O_3$ [MH]$^{+}$ calcd 367.1264; found 367.1269; LC-MS t_R: 3.2 min; HPLC t_R: 6.1 min, > 99%.

***N*-(2-(Hydroxyamino)-2-oxo-1-(3',4',5'-trifluoro-[1,1'-biphenyl]-4-yl)ethyl)propionamide (6b).** Compound **5b** (180 mg, 0.51 mmol) was converted to the corresponding hydroxamic acid according to General Procedure D to give 156 mg (86%) of an oily white solid. ^{1}H NMR (DMSO-d_6) δ 11.01 (s, 1H), 9.01 (s, 1H), 8.61 (d, J = 8.4 Hz, 1H), 7.73–7.60 (m, 4H), 7.49 (d, J = 8.3 Hz, 2H), 5.42 (d, J = 8.4 Hz, 1H), 2.23 (q, J = 7.5 Hz, 2H), 0.98 (t, J = 7.6 Hz, 3H); ^{19}F NMR (DMSO-d_6) δ -134.92 (d, J = 21.7 Hz), -163.52 (dd, J = 21.8/21.8 Hz); ^{13}C NMR (DMSO-d_6) δ 172.9, 166.6, 150.7 (ddd, J_{CF} = 246.6/9.7/4.1 Hz), 139.5, 139.9–136.8 (m), 136.8–136.3 (m), 136.2, 127.7, 126.8,

111.7–110.9 (m), 53.4, 28.1, 9.9; *m/z* HRMS (TOF ES$^+$) $C_{17}H_{16}F_3N_2O_3$ [MH]$^+$ calcd 353.1108; found 353.1107; LC-MS t_R: 3.2 min; HPLC t_R: 5.9 min, > 99%.

3,3,3-Trifluoro-*N*-(2-(hydroxyamino)-2-oxo-1-(3',4',5'-trifluoro-[1,1'-biphenyl]-4-yl)ethyl)propanamide (6c). Compound **5c** (50 mg, 0.12 mmol) was converted to the title compound according to General Procedure D, to give 20 mg (40%) of colourless oil. ^{1}H NMR (DMSO-d_6) δ 11.11 (s, 1H), 9.18 (d, J = 8.2 Hz, 1H), 9.12 (s, 1H), 7.76–7.66 (m, 4H), 7.48 (d, J = 8.3 Hz, 2H), 5.43 (d, J = 8.2 Hz, 1H), 3.46 (app. Q, J = 11.2 Hz, 2H); ^{19}F NMR (DMSO-d_6) δ -61.40, -134.90 (d, J = 21.8 Hz), -163.41 (dd, J = 21.7/21.7 Hz); ^{13}C NMR (DMSO-d_6) δ 165.9, 162.5 (q, J_{CF} = 3.5 Hz), 150.6 (ddd, J_{CF} = 246.6/9.7/4.2 Hz), 138.8, 138.4 (dt, J_{CF} = 248.6/15.4 Hz), 136.6–136.3 (m), 136.4, 127.4, 126.9, 126.6–120.8 (m), 111.5–111.1 (m), 53.5 39.5–38.5 (m)*; *m/z* HRMS (TOF ES$^+$) $C_{17}H_{13}F_6N_2O_3$ [MH]$^+$ calcd 407.0825; found 407.0835; LC-MS t_R: 3.2 min; HPLC t_R: 6.4 min, 96%. Carbon resonance denoted with * is under the DMSO reference signal.

2,3,3,3-Tetrafluoro-*N*-(2-(hydroxyamino)-2-oxo-1-(3',4',5'-trifluoro-[1,1'-biphenyl]-4-yl)ethyl)propanamide (6d). Compound **5d** (250 mg, 0.59 mmol) was converted to the title compound according to General Procedure D. The diastereomers were separated by FCC as white solids; **6d-a** (65 mg) and **6d-b** (63 mg). Diastereomer **6d-a**: ^{1}H NMR (DMSO-d_6) δ 11.16 (s, 1H), 9.55 (d, J = 7.9 Hz, 1H), 9.18 (s, 1H), 7.78–7.65 (m, 4H), 7.48 (d, J = 8.3 Hz, 2H), 5.87 (dq, J = 44.9/6.7 Hz, 1H), 5.47 (d, J = 7.8 Hz, 1H); ^{19}F NMR (DMSO-d_6) δ -75.07 (d, J = 13.0 Hz), -134.88 (d, J = 21.7 Hz), -163.31 (dd, J = 21.8/21.8 Hz), -204.88 (q, J = 13.0 Hz); ^{13}C NMR (DMSO-d_6) δ 165.3, 160.4–159.9 (m), 150.6 (ddd, J_{CF} = 246.6/9.8/4.3 Hz), 138.4 (dt, J_{CF} = 249.4/16.1 Hz), 137.9, 136.6, 136.5–136.1 (m), 127.4, 127.0, 121.0 (app. d, J_{CF} = 281.6 Hz), 111.5–111.0 (m), 83.7 (dd, J_{CF} = 189.8/33.3 Hz), 53.7; *m/z* HRMS (TOF ES$^+$) $C_{17}H_{12}F_7N_2O_3$ [MH]$^+$ calcd 425.0731; found 425.0738; LC-MS t_R: 3.3 min; HPLC t_R: 6.7 min, > 99%; Diastereomer **6d-b**: ^{1}H NMR (DMSO-d_6) δ 11.12 (s, 1H), 9.50 (d, J = 8.0 Hz, 1H), 9.19 (s, 1H), 7.80–7.63 (m, 4H), 7.51 (d, J = 8.3 Hz, 2H), 5.88 (dq, J = 44.9/6.7 Hz, 1H), 5.45 (d, J = 8.0 Hz, 1H); ^{19}F NMR (DMSO-d_6) δ -75.16 (d, J = 13.0 Hz), -134.87 (d, J = 21.8 Hz), -163.31 (dd, J = 21.7/21.7 Hz), -204.97 (q, J =

12.9 Hz); ^{13}C NMR (DMSO-d_6) δ 165.3, 160.3–160.0 (m), 150.6 (ddd, J_{CF} = 246.9/9.8/4.2 Hz), 138.4 (dt, J_{CF} = 249.6/15.7 Hz), 138.1, 136.6, 136.5–135.6 (m), 127.5, 127.0, 121.1 (qd, J_{CF} = 282.0/26.5 Hz), 111.5–111.0 (m), 83.9 (ddd, J_{CF} = 190.6/66.8/33.5 Hz), 53.7; *m/z* HRMS (TOF ES$^+$) $C_{17}H_{12}F_7N_2O_3$ [MH]$^+$ calcd 425.0731; found 425.0745; LC-MS t_R: 3.3 min; HPLC t_R: 6.8 min, 98%;

2,2,3,3,3-Pentafluoro-*N*-(2-(hydroxyamino)-2-oxo-1-(3',4',5'-trifluoro-[1,1'-biphenyl]-4-yl)ethyl)propanamide (6e). Compound **5e** (160 mg, 0.36 mmol) was converted to the title compound according to General Procedure D to give 80 mg (50%) of yellow solid. ^{1}H NMR (DMSO-d_6) δ 11.10 (s, 1H), 10.28 (d, J = 5.3 Hz, 1H), 9.17 (s, 1H), 7.78–7.68 (m, 4H), 7.54 (d, J = 8.4 Hz, 2H), 5.50 (d, J = 4.1 Hz, 1H); ^{19}F NMR (DMSO-d_6) δ -82.09, -120.88 (d, J = 7.3 Hz), -134.85 (d, J = 21.7 Hz), -163.25 (dd, J = 21.7/21.7 Hz); ^{13}C NMR (DMSO-d_6) δ 164.9, 156.9 (t, J_{CF} = 26.3 Hz), 150.6 (ddd, J_{CF} = 246.6/9.4/4.1 Hz), 139.9–136.9 (m), 136.8, 136.5–136.2 (m), 128.2, 127.0, 120.0–115.3 (m), 111.6–110.7 (m), 107.2–105.6 (m), 54.4; *m/z* HRMS (TOF ES$^+$) $C_{17}H_{11}F_8N_2O_3$ [MH]$^+$ calcd 443.0636; found 443.0643; LC-MS t_R: 6.7 min; HPLC t_R: 7.2 min, 99%.

***N*-(2-(Hydroxyamino)-2-oxo-1-(3',4',5'-trifluoro-[1,1'-biphenyl]-4-yl)ethyl)cyclopropanecarboxamide (6f).** Compound **5f** (150 mg, 0.41 mmol) was converted to the corresponding hydroxamic acid according to General Procedure D to give 120 mg (80%) of white solid. ^{1}H NMR (DMSO-d_6) δ 11.02 (s, 1H), 9.02 (s, 1H), 8.95 (d, J = 8.5 Hz, 1H), 7.78–7.62 (m, 4H), 7.51 (d, J = 8.3 Hz, 2H), 5.45 (d, J = 8.5 Hz, 1H), 2.00–1.78 (m, 1H), 0.73–0.60 (m, 4H); ^{19}F NMR (DMSO-d_6) δ -134.92 (d, J = 21.7 Hz), -163.50 (dd, J = 21.8/21.8 Hz); ^{13}C NMR (DMSO-d_6) δ 172.6, 166.7, 150.7 (ddd, J = 246.6/9.6/4.1 Hz), 139.5, 140.1–136.9 (m), 136.9–136.4 (m), 136.3, 127.7, 126.9, 111.5–110.9 (m), 53.6, 13.3, 6.8, 6.7; *m/z* HRMS (TOF ES$^+$) $C_{18}H_{16}F_3N_2O_3$ [MH]$^+$ calcd 365.1108; found 365.1107; LC-MS t_R: 3.3 min; HPLC t_R: 7.1 min, > 99%.

***N*-(2-(Hydroxyamino)-2-oxo-1-(3',4',5'-trifluoro-[1,1'-biphenyl]-4-yl)ethyl)cyclobutanecarboxamide (6g).** Compound **5g** (200 mg, 0.53 mmol) was converted to the

corresponding hydroxamic acid according to General Procedure D to give 129 mg (64%) of white solid. ^{1}H NMR (DMSO-d_6) δ 11.01 (s, 1H), 9.01 (s, 1H), 8.46 (d, J = 8.4 Hz, 1H), 7.77–7.60 (m, 4H), 7.48 (d, J = 8.3 Hz, 2H), 5.42 (d, J = 8.4 Hz, 1H), 3.30–3.19 (m, 1H), 2.17–1.67 (m, 6H); ^{19}F NMR (DMSO-d_6) δ -134.93 (d, J = 21.8 Hz), -163.52 (dd, J = 21.8/21.8 Hz); ^{13}C NMR (DMSO-d_6) δ 173.9, 166.7, 150.7 (ddd, J_{CF} = 246.6/9.6/4.0 Hz), 139.5, 139.9–136.9 (m), 136.9–136.5 (m), 136.3, 127.7, 126.9, 111.6–110.9 (m), 53.5, 38.3, 24.7, 24.6, 17.9; *m/z* HRMS (TOF ES$^+$) $C_{19}H_{18}F_3N_2O_3$ [MH]$^+$ calcd 379.1264; found 379.1265; LC-MS t_R: 3.3 min.

***N*-(2-(Hydroxyamino)-2-oxo-1-(3',4',5'-trifluoro-[1,1'-biphenyl]-4-yl)ethyl)cyclopentanecarboxamide (6h).** Compound **5h** (60 mg, 0.15 mmol) was converted to the title compound according to General Procedure D, to give 20 mg (33%) of white solid. ^{1}H NMR (DMSO-d_6) δ 11.02 (d, J = 1.2 Hz, 1H), 9.03 (d, J = 1.3 Hz, 1H), 8.59 (d, J = 8.4 Hz, 1H), 7.74–7.65 (m, 4H), 7.49 (d, J = 8.3 Hz, 2H), 5.42 (d, J = 8.4 Hz, 1H), 2.91–2.75 (m, 1H), 1.86–1.42 (m, 8H); ^{19}F NMR (DMSO-d_6) δ -134.93 (d, J = 21.8 Hz), -163.53 (dd, J = 21.8/21.8 Hz); ^{13}C NMR (DMSO-d_6) δ 175.2, 166.5, 150.6 (ddd, J_{CF} = 246.6/9.6/4.1 Hz), 139.5, 137.0, 136.7–136.4 (m), 136.1, 127.5, 126.8, 111.5–110.9 (m), 53.3, 43.5, 30.07, 29.98, 25.77, 25.75; *m/z* HRMS (TOF ES$^+$) $C_{20}H_{20}F_3N_2O_3$ [MH]$^+$ calcd 393.1421; found 393.1431; LC-MS t_R: 3.6 min; HPLC t_R: 6.5 min, 95%.

***N*-(2-(hydroxyamino)-2-oxo-1-(3',4',5'-trifluoro-[1,1'-biphenyl]-4-yl)ethyl)cyclohexanecarboxamide (6i).** Methyl 2-(cyclohexanecarboxamido)-2-(3',4',5'-trifluoro-[1,1'-biphenyl]-4-yl)acetate (**5i**) (40 mg, 0.10 mmol) was converted to the title compound according to General Procedure D, to give 15 mg (37%) of white solid. ^{1}H NMR (DMSO-d_6) δ 11.01 (s, 1H), 9.02 (s, 1H), 8.47 (d, J = 8.4 Hz, 1H), 7.76–7.58 (m, 4H), 7.50 (d, J = 8.1 Hz, 2H), 5.42 (d, J = 8.4 Hz, 1H), 2.48–2.29 (m, 1H), 1.78–1.52 (m, 5H), 1.47–0.98 (m, 5H); ^{19}F NMR (DMSO-d_6) δ -134.94 (d, J = 21.6 Hz), -163.61 (dd, J = 21.6/21.6 Hz); ^{13}C NMR (DMSO-d_6) δ 175.1, 166.6, 150.6 (ddd, J_{CF} = 246.6/9.7/4.0 Hz), 140.1–136.8 (m), 139.5, 136.8–136.3 (m), 136.1, 127.5, 126.7,

111.6–110.8 (m), 53.1, 43.3, 29.3, 29.1, 25.5, 25.2 (2C); *m/z* HRMS (TOF ES$^+$) $C_{21}H_{22}F_3N_2O_3$ [MH]$^+$ calcd 407.1577; found 407.1589; LC-MS t_R: 3.7 min; HPLC t_R: 6.9 min, > 99%.

***N*-(2-(Hydroxyamino)-2-oxo-1-(3',4',5'-trifluoro-[1,1'-biphenyl]-4-yl)ethyl)tetrahydro-2*H*-pyran-4-carboxamide (6j).** Methyl 2-(tetrahydro-2*H*-pyran-4-carboxamido)-2-(3',4',5'-trifluoro-[1,1'-biphenyl]-4-yl)acetate (**5j**) (100 mg, 0.25 mmol) was converted to the title compound according to General Procedure D, to give 65 mg (65%) of beige solid. ^{1}H NMR (DMSO-d_6) δ 11.03 (s, 1H), 9.03 (d, J = 1.0 Hz, 1H), 8.63 (d, J = 8.4 Hz, 1H), 7.74–7.65 (m, 4H), 7.49 (d, J = 8.3 Hz, 2H), 5.41 (d, J = 8.4 Hz, 1H), 3.93–3.76 (m, 2H), 3.36–3.19 (m, 2H), 2.71–2.59 (m, 1H), 1.66–1.41 (m, 4H); ^{19}F NMR (DMSO-d_6) δ -134.92 (d, J = 21.8 Hz), -163.50 (dd, J = 21.7/21.7 Hz); ^{13}C NMR (DMSO-d_6) δ 174.0, 166.6, 150.7 (ddd, J_{CF} = 246.4/9.8/4.0 Hz), 139.4, 137.2, 136.8–136.5 (m), 136.3, 127.6, 126.9, 111.5–111.1 (m), 66.54, 66.52, 53.4, 40.3, 29.1, 29.0; *m/z* HRMS (TOF ES$^+$) $C_{20}H_{20}F_3N_2O_4$ [MH]$^+$ calcd 409.1370; found 409.1396; LC-MS t_R: 3.4 min; HPLC t_R: 5.9 min, > 99%.

***N*-(2-(Hydroxyamino)-2-oxo-1-(3',4',5'-trifluoro-[1,1'-biphenyl]-4-yl)ethyl)adamantane-1-carboxamide (6k).** Compound **5k** (140 mg, 0.31 mmol) was converted to the title compound according to General Procedure D, to give 80 mg (56%) of beige solid. ^{1}H NMR (DMSO-d_6) δ 11.03 (s, 1H), 9.09 (s, 1H), 7.74–7.63 (m, 5H), 7.50 (d, J = 8.3 Hz, 2H), 5.42 (d, J = 8.0 Hz, 1H), 2.02–1.93 (m, 3H), 1.89–1.78 (m, 6H), 1.73–1.62 (m, 6H); ^{19}F NMR (DMSO-d_6) δ -134.92 (d, J = 21.8 Hz), -163.52 (dd, J = 21.8/21.8 Hz); ^{13}C NMR (DMSO-d_6) δ 176.3, 166.5, 150.6 (ddd, J_{CF} = 246.6/9.7/4.2 Hz), 139.8–136.8 (m), 139.5, 136.9–136.3 (m), 136.1, 127.4, 126.8, 111.6–110.8 (m), 53.2, 40.0, 38.4, 36.0, 27.7; *m/z* HRMS (TOF ES$^+$) $C_{25}H_{26}F_3N_2O_3$ [MH]$^+$ calcd 459.1890; found 459.1872; LC-MS t_R: 3.9 min; HPLC t_R: 7.8 min, 97%.

***N*-(2-(Hydroxyamino)-2-oxo-1-(3',4',5'-trifluoro-[1,1'-biphenyl]-4-yl)ethyl)-3,3-dimethylbutanamide (6l).** Methyl 2-(3,3-dimethylbutanamido)-2-(3',4',5'-trifluoro-[1,1'-biphenyl]-4-yl)acetate (**5l**) (100 mg, 0.25 mmol) was converted to the title compound according to General Procedure D, to give 75 mg (75%) of white solid. ^{1}H NMR (DMSO-d_6) δ 11.09 (s, 1H), 9.10 (s,

1H), 8.62 (d, J = 8.3 Hz, 1H), 7.85–7.73 (m, 4H), 7.59 (d, J = 8.3 Hz, 2H), 5.53 (d, J = 8.3 Hz, 1H), 2.31–2.12 (m, 2H), 1.03 (s, 9H); ^{19}F NMR (DMSO-d_6) δ -134.94 (d, J = 21.7 Hz), -163.55 (dd, J = 21.7/21.7 Hz); ^{13}C NMR (DMSO-d_6) δ 170.7, 166.6, 150.61 (ddd, J_{CF} = 246.3/9.7/4.1 Hz), 139.8–136.7 (m), 139.5, 136.74–136.32 (m), 136.0, 127.6, 126.7, 111.4–110.9 (m), 53.2, 47.9, 30.6, 29.7; *m/z* HRMS (TOF ES$^+$) $C_{20}H_{22}F_3N_2O_3$ [MH]$^+$ calcd 395.1577; found 395.1590; LC-MS t_R: 3.3 min; HPLC t_R: 6.9 min, 97%.

2-(2-Cyclopropylacetamido)-*N*-hydroxy-2-(3',4',5'-trifluoro-[1,1'-biphenyl]-4-yl)acetamide (6m). Compound **5m** (60 mg, 0.16 mmol) was converted to the title compound according to General Procedure D, to give 26 mg (43%) of pale yellow solid. ^{1}H NMR (DMSO-d_6) δ 11.04 (s, 1H), 9.05 (s, 1H), 8.57 (d, J = 8.5 Hz, 1H), 7.75–7.66 (m, 4H), 7.50 (d, J = 8.3 Hz, 2H), 5.44 (d, J = 8.4 Hz, 1H), 2.21–2.05 (m, 2H), 1.01–0.87 (m, 1H), 0.47–0.31 (m, 2H), 0.22–0.02 (m, 2H); ^{19}F NMR (DMSO-d_6) δ -134.93 (d, J = 21.8 Hz), -163.51 (dd, J = 21.8/21.8 Hz); ^{13}C NMR (DMSO-d_6) δ 171.4, 166.5, 152.13–149.08 (m), 139.5, 137.1, 136.8–136.2 (m), 136.1, 127.5, 126.8, 111.4–111.0 (m), 53.2, 7.8, 4.1, 4.0; *m/z* HRMS (TOF ES$^+$) $C_{19}H_{18}F_3N_2O_3$ [MH]$^+$ calcd 379.1264; found 379.1274; LC-MS t_R: 3.5 min; HPLC t_R: 6.4 min, 95%.

2-(2-Cyclobutylacetamido)-*N*-hydroxy-2-(3',4',5'-trifluoro-[1,1'-biphenyl]-4-yl)acetamide (6n). Compound **5n** (90 mg, 0.23 mmol) was converted to the title compound according to General Procedure D, to give 20 mg (22%) of yellow solid. ^{1}H NMR (DMSO-d_6) δ 11.00 (s, 1H), 9.03 (s, 1H), 8.60 (d, J = 8.4 Hz, 1H), 7.77–7.63 (m, 4H), 7.47 (d, J = 8.3 Hz, 2H), 5.40 (d, J = 8.4 Hz, 1H), 2.60–2.51 (m, 1H), 2.34 (d, J = 7.4 Hz, 2H), 2.03–1.91 (m, 2H), 1.83–1.73 (m, 2H), 1.71–1.61 (m, 2H); ^{19}F NMR (DMSO-d_6) δ -134.94 (d, J = 21.8 Hz), -163.52 (dd, J = 21.8/21.8 Hz); ^{13}C NMR (DMSO-d_6) δ 171.0, 166.5, 150.6 (ddd, J_{CF} = 246.6/9.6/4.1), 139.5, 137.6–136.9 (m), 136.8–136.3 (m), 136.0, 127.5, 126.7, 112.9–109.8 (m), 53.2, 41.7, 32.7, 27.7, 27.6, 18.1; *m/z* HRMS (TOF ES$^+$) $C_{20}H_{20}F_3N_2O_3$ [MH]$^+$ calcd 393.1421; found 393.1433; LC-MS t_R: 3.6 min; HPLC t_R: 6.7 min, 97%.

2-(2-Cyclopentylacetamido)-*N*-hydroxy-2-(3',4',5'-trifluoro-[1,1'-biphenyl]-4-yl)acetamide (6o). Compound **5o** (130 mg, 0.32 mmol) was converted to the title compound according to General Procedure D, to give 40 mg (31%) of white solid. ^{1}H NMR (DMSO-d_6) δ 11.02 (s, 1H), 9.03 (s, 1H), 8.61 (d, J = 8.4 Hz, 1H), 7.75–7.64 (m, 4H), 7.49 (d, J = 8.3 Hz, 2H), 5.43 (d, J = 8.3 Hz, 1H), 2.27–2.18 (m, 2H), 2.17–2.05 (m, 1H), 1.72–1.37 (m, 6H), 1.18–1.06 (m, 2H); ^{19}F NMR (DMSO-d_6) δ -134.93 (d, J = 21.7 Hz), -163.53 (dd, J = 21.7/21.7 Hz); ^{13}C NMR (DMSO-d_6) δ 171.7, 166.5, 150.6 (ddd, J_{CF} = 246.7/9.8/4.1 Hz), 139.6–136.8 (m), 139.5, 136.7–136.4 (m), 136.1, 127.6, 126.7, 111.6–110.8 (m), 53.3, 40.9, 36.8, 31.9, 31.8, 24.50, 24.49; *m/z* HRMS (TOF ES$^+$) $C_{21}H_{22}F_3N_2O_3$ [MH]$^+$ calcd 407.1577; found 407.1593; LC-MS t_R: 3.6 min; HPLC t_R: 6.8 min, 97%.

2-(2-Cyclohexylacetamido)-*N*-hydroxy-2-(3',4',5'-trifluoro-[1,1'-biphenyl]-4-yl)acetamide (6p). Compound **5p** (80 mg, 0.19 mmol) was converted to the title compound according to General Procedure D, to give 24 mg (30%) of white solid. ^{1}H NMR (DMSO-d_6) δ 11.01 (s, 1H), 9.02 (s, 1H), 8.61 (d, J = 8.4 Hz, 1H), 7.74–7.64 (m, 4H), 7.49 (d, J = 8.3 Hz, 2H), 5.43 (d, J = 8.3 Hz, 1H), 2.11 (d, J = 6.8 Hz, 2H), 1.76–1.49 (m, 6H), 1.25–1.03 (m, 3H), 1.03–0.80 (m, 2H); ^{19}F NMR (DMSO-d_6) δ -134.94 (d, J = 21.8 Hz), -163.52 (dd, J = 21.7/21.7 Hz); ^{13}C NMR (DMSO-d_6) δ 170.7, 166.6, 152.1–149.2 (m), 139.5–136.9 (m), 139.4, 136.9–136.2 (m), 136.1, 127.6, 126.8, 111.4–111.0 (m), 53.3, 42.7, 34.9, 32.6, 32.5, 25.9, 25.7 (2C); *m/z* HRMS (TOF ES$^+$) $C_{22}H_{24}F_3N_2O_3$ [MH]$^+$ calcd 421.1734; found 421.1747; LC-MS t_R: 3.7 min; HPLC t_R: 7.1 min, > 99%.

2-(2-(Cuban-1-yl)acetamido)-*N*-hydroxy-2-(3',4',5'-trifluoro-[1,1'-biphenyl]-4-yl)acetamide (6q). Compound **5q** (200 mg, 0.46 mmol) was converted to the title compound according to General Procedure D, to give 95 mg (47%) of white solid. ^{1}H NMR (DMSO-d_6) δ 11.01 (s, 1H), 9.03 (s, 1H), 8.56 (d, J = 8.3 Hz, 1H), 7.75–7.65 (m, 4H), 7.47 (d, J = 8.3 Hz, 2H), 5.41 (d, J = 8.2 Hz, 1H), 4.01–3.95 (m, 1H), 3.88–3.75 (m, 6H), 2.60–2.51 (m, 2H); ^{19}F NMR (DMSO-d_6) δ -134.9 (d, J = 21.8 Hz), -163.5 (dd, J = 21.7/21.7 Hz); ^{13}C NMR (DMSO-d_6) δ 169.4,

166.5, 150.6 (ddd, J_{CF} = 246.8/9.7/4.0 Hz), 139.7–136.9, 139.5, 136.7–136.4 (m), 136.0, 127.5, 126.7, 111.4–110.9 (m), 55.3, 53.3, 48.5, 47.2, 43.5, 38.8; *m/z* HRMS (TOF ES$^+$) $C_{24}H_{20}F_3N_2O_3$ [MH]$^+$ calcd 441.1421; found 441.1434; LC-MS t_R: 3.4 min; HPLC t_R: 7.3 min, 98%.

2-(2-(Bicyclo[2.2.1]heptan-2-yl)acetamido)-*N*-hydroxy-2-(3',4',5'-trifluoro-[1,1'-biphenyl]-4-yl)acetamide (6r). Compound **5r** (90 mg, 0.21 mmol) was converted to the title compound according to General Procedure D, to give 34 mg (38%) of white solid. ^{1}H NMR (DMSO-d_6) δ 11.02 (d, J = 5.1 Hz, 1H), 9.04 (d, J = 3.6 Hz, 1H), 8.61 (dd, J = 8.3/2.7 Hz, 1H), 7.79–7.61 (m, 4H), 7.49 (dd, J = 8.3/3.3 Hz, 2H), 5.43 (d, J = 8.3 Hz, 1H), 2.25–2.02 (m, 3H), 1.94–1.72 (m, 2H), 1.47–1.25 (m, 4H), 1.14–0.95 (m, 4H); ^{19}F NMR (DMSO-d_6) δ -134.92 (d, J = 21.7 Hz), -163.54 (dd, J = 21.7/21.7 Hz); ^{13}C NMR (DMSO-d_6) δ 171.38, 171.36*, 166.6, 150.6 (ddd, J_{CF} = 246.5/9.6/4.0 Hz), 139.8–136.8 (m), 139.51, 139.48*, 136.7–136.4 (m), 136.1, 127.6, 126.76, 126.73*, 111.5–110.9 (m), 53.3, 41.84, 41.80*, 40.5, 40.4*, 38.8, 38.7, 37.0, 36.18, 36.13*, 34.91, 34.87*, 29.46, 29.41*, 28.43, 28.37*; *m/z* HRMS (TOF ES$^+$) $C_{23}H_{24}F_3N_2O_3$ [MH]$^+$ calcd 433.1734; found 433.1741; LC-MS t_R: 3.7 min; HPLC t_R: 7.4 min, 96%. All signals with an * correspond to the 2nd conformer (50:50).

Biology. *Protein Expression and Purification.* DNA coding for *Pv*-M1 (residues 195–1097) and *Pv*-M17 (residues 203–621) with C-terminal His6 tags were chemically synthesized by DNA2.0 using codons optimized for gene expression in *Escherichia coli*, and provided in the pJ404 vector for expression. Cloning of C-terminally His6 tagged expression vectors for *Pf*-M1 (residues 195–1085) and *Pf*-M17 (residues 85–605) were described previously.[24, 25]

The four plasmodial aminopeptidases were expressed by the autoinduction method in *Escherichia coli* BL21(DE3). Cells were lysed by sonication in PBS pH 8.0, 300 mM NaCl, 5% glycerol, 20 mM imidazole. Clarified lysates were bound to a Ni-NTA-agarose column in nickel-affinity buffer (PBS pH8.0, 300 mM NaCl, 5% glycerol, 20 mM imidazole), and eluted in nickel-affinity buffer supplemented with 250 mM imidazole. The proteins were further purified by size exclusion chromatography on Superdex S200 10/300 gel filtration column in either 50 mM HEPES

pH 8.0, 300 mM NaCl (*Pv*-M17 and *Pf*-M17) or the same buffer supplemented with 5% glycerol (*Pv*-M1 and *Pf*-M1).

Partially purified IRAP was provided as a kind gift from Dr Siew Chai and Peta Burns from Monash University. APN was purified from the supernatant of a stably transfected HEK293S GnT1^{-} cell line, which was a kind gift from Professor James Rini from the University of Toronto, Canada, using methods reported previously.[41]

Determination of Aminopeptidase Kinetic Parameters and Inhibition Constants. The ability of compounds to inhibit aminopeptidase activity was assessed by fluorescence assays using the fluorogenic peptide *L*-Leucine-7-amido-4-methylcoumarin hydrochloride (H-Leu-NHMec) (Sigma L2145) as substrate. The reactions were carried out in white 384–well plates, 50 µL total volume at 37°C using a spectrofluorimeter (BMG FLUOstar) with excitation at 355 nm and emission at 460 nm. The fluorescence signal was continuously monitored until a final steady state velocity, *v*, was obtained. Inhibition constants were calculated in biological triplicate from three different protein preparations. Kinetic parameters were determined for each preparation of protein in experimental triplicate.

For determination of kinetic parameters, enzyme was first added to 100 mM Tris–HCl, pH 8.0 (supplemented with 1 mM CoCl2 for *Pv*-M17 or 2 mM CoCl2 for *Pf*-M17) for 10 minutes prior to the addition of substrate. Initial rates were obtained at 37 °C over a range of substrate concentrations spanning K_m (0.5–500 µM) and at fixed enzyme concentration: 20 nM *Pf*-M1, 10 nM *Pv*-M1, 150 nM *Pf*-M17, 125 nM *Pv*-M17. Calculations of Michaelis-Menten constants (K_m) were performed using GraphPad Prism.

Previous examination of compound *Pf*-M1 and *Pf*-M17 inhibitory activity was performed using the Dixon method.[15, 17, 20, 42, 43] However, first pass screening of the current inhibitor series demonstrated that compound inhibition constants were approaching, or indeed passing, the concentration of enzyme used in the assays. We therefore re-structured our method of compound examination to use a modified Morrison equation for tight-binding inhibitors.[27, 28] For determination

of the Morrison inhibition constant (K_i enzymes were pre-incubated in 100 mM Tris–HCl, pH 8.0 (supplemented with 1 mM CoCl2 for *Pv*-M17 or 2 mM CoCl2 for *Pf*-M17) and the inhibitors for 20 min prior to the addition of substrate (20 μM for *Pf*-M1, 40 μM for *Pv*-M1, 10 μM for *Pf*-M17, 10 μM for *Pv*-M17). Substrate (L-Leucine-7-amido-4-methylcoumarin) concentrations were selected to allow sensitive detection of enzyme activity while not exceeding the K_m for each enzyme. First pass inhibition assays were conducted with a compound concentration range of 500 nM – 500 pM. The concentration range was then adjusted for the second pass assay to obtain a complete inhibition curve (0% – 100 %) in biological triplicate. The K_i values were calculated by plotting the initial rates versus inhibitor concentration, and fitting to the Morrison equation for tight-binding inhibitors in GraphPad Prism (non-linear regression method).

To assess possible off-target activity, ability of **6l** to inhibit a panel of matrix metalloproteinases (MMPs) was examined. Purified MMPs were activated using 1 mM 4-aminophenylmercuric acetate in buffer containing 50 mM HEPES, 150 mM NaCl, 5 mM $CaCl_2$, pH 7.0 for 1 h at room temperature, at working MMP concentrations of 1 μM (MMP2, 9 or 13) or 10 μM (MMP7 or 8). Each activated MMP was incubated at 2–20 nM concentrations with increasing inhibitor concentrations (0.1 pM–100 μM) of **6l**, Marimastat, or Tosedostat in fluorimetry assay buffer composed of 100 mM Tris-HCl, 100 mM NaCl, 10 mM $CaCl_2$, 0.15% Brij-35, pH 7.5 for 1 h at room temperature. Quenched fluorescent (QF)-24 substrate (ChinaPeptides Co. Ltd., Shanghai, China) was dissolved in DMSO and diluted to 10 μM working concentrations in fluorimetry assay Buffer. QF assays were performed by incubating each MMP-inhibitor solution with 1 μM QF24 substrate at 37°C and measuring fluorescence at excitation and emission wavelengths of 320 and 405 nm, respectively, at 1-minute intervals over 1 h using a fluorescence plate reader (POLARStar, OPTIMA, BMG Labtech, Ortenberg, Germany). IC_{50} values for each inhibitor were calculated by plotting log(inhibitor concentration) vs. activity rate (pmol of QF24 substrate cleaved/h) and applying the 4-parameter Hill equation (GraphPad Prism 5.0, La Jolla, CA). Each MMP was assayed with all inhibitors in 3 independent experiments.

Inhibition of APN and IRAP was performed using the same aminopeptidase assay used for the Plasmodial enzymes. Briefly, purified APN or partially-purified IRAP was added to assay buffer (100 mM Tris pH 8) and incubated with increasing concentrations of compound for 10 min at 37 °C. Triplicate reactions were started with the addition of L-Leucine-7-amido-4-methylcoumarin (final concentration 25 μM) and monitored for 30 mins. Data was processed as described above.

Compound Washout Experiments.

To assess reversibility of **6k** binding to *Pf*-M17, wash out experiments were performed. *Pf*-M17 at 20 μM was incubated with either **6k** (150 μM), bestatin (150 μM), EDTA (2 mM), or buffer only (50 mM HEPES pH8, 300 mM NaCl) at 4 °C overnight. Inhibitor concentrations were selected to ensure 100% saturation, and EDTA to complete remove metal cofactors (EDTA inhibition previously reported in [31]). Protein samples were then washed with buffer (50 mM HEPES pH8, 300 mM NaCl) by consecutive 10-fold concentration and dilution steps for up to 7 hours. For analysis of activity, final washed *Pf*-M17 samples were incubated in assay buffer (1 mM MnCl2, 100 mM Tris pH 8.0) for 10 mins prior to the addition of substrate (final concentration 25 μM). Fluorescence was monitored for 30 mins.

Structural Biology. *Crystallisation, Data Collection, and Refinement.* *Pf*-M1 and *Pf*-M17 were co-crystallised with bound inhibitors by the hanging-drop method, using previously established protocols.[24, 25] For *Pf*-M1, purified protein was concentrated to 5.0 mg/mL and mixed with the appropriate compound (40 mM in 100% DMSO) to a final ligand concentration of 1 mM. Crystals grew in 20-30 % PEG8000, 0.1 M Tris pH 7.5–8.5, 0.2 M $MgCl_2$, 10% glycerol, and, where necessary were subjected to an additional overnight compound soak (mother liquor supplemented with 1 mM ligand) before being harvested for data collection. *Pf*-M17 was concentrated to 10 mg/mL and co-crystallised with a final ligand concentration of 1 mM in 30–40% PEG400, 0.1 M Tris pH 7.5–8.5, 0.2 M Li_2SO_4. Where appropriate, *Pf*-M17 crystals were soaked

overnight in mother liquor supplemented with 1 mM ligand and 1 mM $ZnSO_4$ before being harvested for data collection.

Crystals were snap frozen in liquid nitrogen, and data were collected 100K using synchrotron radiation at the Australian Synchrotron beamlines 3BM1[44] and 3ID1. For *Pf*-M17, data were collected from two to three wedges of the same crystal, which were merged after integration. Data were processed using iMosflm[45] or XDS [46], and Aimless[47] as part of the CCP4i program suite.[48] The structures were solved by molecular replacement in Phaser[49] using the structure of unliganded *Pf*-M1 (RCSB ID 3EBG) or *Pf*-M17 (RCSB ID 3KQZ) as the search models. The structures were refined using Phenix[50], with 5% of reflections set aside for calculation of R_{free}. Between refinement cycles, the protein structure, solvent, and inhibitors were manually built into $2F_o$–F_c and F_o–F_c electron density maps using COOT[51, 52], with restraint files generated by Phenix where necessary. The coordinates and structure factors are available from the Protein Data Bank with PDB Accession codes *Pf*-M1: 6EA1 (**6d-a**), 6EA2 (**6h**), 6EAA (**6i**), 6EAB (**6j**), 6EE3 (**6k**), 6EE4 (**6m**), 6EE6 (**6o**), 6EED (**6p**) and *Pf*-M17: 6EE2 (**6i**), 6EEE (**6k**).

***P. falciparum* Growth Inhibition Assay.**[53] Compounds were dissolved in 100% DMSO to a final stock concentration of 10 mM. Stock solutions of reference drugs (chloroquine, artesunate, puromycin, pyronaridine, dihydroartemisinin and pyrimethamine) were prepared at 2.5 mM (dihydroartemisinin and artesunate) or 10 mM (puromycin and pyrimethamine) in 100% DMSO. Chloroquine and pyronaridine were dissolved in water to 30 mM concentration and then 1:3 in 100% DMSO to 10 mM prior to performing serial dilutions. Puromycin (5 μM) and 0.4% DMSO were used as positive and negative controls, respectively. The compounds were tested in 16-point dose-response against the 3D7 and Dd2 strains of *Plasmodium falciparum* using three concentrations per log dose at a final concentration range of 40 μM – 0.4 nM. Stock solutions were serially diluted in 100% DMSO, before dilution 1:25 in water, then 1:10 in the final assay volume, to give a final assay top concentration of 40 μM. Reference compounds were tested using 21-point concentration-response range of 40 μM – 0.01 nM (puromycin, pyrimethamine, and chloroquine) or

10 μM – 0.003 nM (dihydroartemisinin and artesunate). The final DMSO concentration in the assay was 0.4% for all compounds except chloroquine and pyronaridine (for which it was in the range 0.27% - 0.40%). The experiment was performed in two biological replicates, each consisting of two technical repeats. Each biological replicate was carried out from independent compound handling processes.

P. falciparum parasites (3D7 and Dd2 strains) were grown in RPMI 1640 supplemented with 25 mM HEPES, 5% AB human male serum, 2.5 mg/ml Albumax II, and 0.37 mM hypoxanthine. Parasites were subjected to two rounds of sorbitol synchronization before undergoing compound treatment. Ring stage parasites were exposed to the compounds in 384-wells imaging CellCarrier microplates (PerkinElmer), as previously described.[53] Plates were incubated for 72h at 37 °C, 90% N_2, 5% CO_2, 5% O_2, then the parasites were stained with 2-(4-amidinophenyl)-1H -indole-6-carboxamidine (DAPI), and imaged using an Opera QEHS micro-plate confocal imaging system (PerkinElmer). Images were analyzed as previously described.[53] Briefly, raw data was normalized using the in-plate positive and negative controls to obtain normalized percent inhibition data, which was then used to calculate IC_{50} values, through a 4-parameter logistic curve fitting in Prism (GraphPad).

HEK293 Cell Viability Assay. Compounds were prepared for the HEK293 viability assay as described above. Human Embryonic Kidney cells (HEK293) were maintained in DMEM medium supplemented with 10% FBS. HEK293 cells were exposed to the compounds in TC-treated 384-wells plates (Greiner) for 72h at 37 °C, 5% CO_2, then the media was removed from the wells and replaced with an equal volume of 44 μM resazurin. After 5-6 hours incubation under standard conditions, the total fluorescence (excitation/emission: 530 nm / 595 nm) was measured using an Envision plate reader (PerkinElmer).

■ ANCILLARY INFORMATION

Supporting Information (PDF)

Supp Figure 1.	Proposed mechanism of hemoglobin digestion and action of hydroxamate inhibitors in *Plasmodium*	S2
Supp Figure 2.	Compound design schematic from substrate analogue to compound **1**	S3
Supp Figure 3.	Binding mode of compound **1** to *Pf*-M1 and *Pf*-M17	S4
Supp Figure 4.	Binding of **6k** is reversible, but possesses a very slow off-rate.	S5
Supp Table 1.	*Pf*-M1–**6da**, **6h**, **6i**, and **6j** Data Collection and Refinement Statistics	S6
Supp Table 2.	*Pf*-M1–**6k**, **6m**, **6o**, and **6p** Data Collection and Refinement Statistics.	S7
Supp Table 3.	*Pf*-M17–**6i**, and **6k** Data Collection and Refinement Statistics.	S8
Supp Table 4:	Activity of **6l** against a panel of matrix metalloproteinases	S9

Molecular-formula strings (CSV)

PDB ID Codes:

Pf-M1–**6d-a** 6EA1

Pf-M1–**6h** 6EA2

Pf-M1–**6i** 6EAA

Pf-M1–**6j** 6EAB

Pf-M1–**6k** 6EE3

Pf-M1–**6m** 6EE4

Pf-M1–**6o** 6EE6

Pf-M1–**6p** 6EED

Pf-M17–**6i** 6EE2

Pf-M17–**6k** 6EEE

Authors will release the atomic coordinates and experimental data upon article publication.

■ AUTHOR INFORMATION

Corresponding Author Information

*S.M.: email, E-mail: Sheena.McGowan@monash.edu. ORCID 0000-0001-6863-1106

* P.J.S.: e-mail, Peter.Scammells@monash.edu. ORCID 0000-0003-2930-895X

Author Contributions

§ N.B.V. and N.D. contributed equally to this work. The manuscript was written through contributions of all authors, and all authors have given approval to the final version of the manuscript.

Notes

The authors declare no competing financial interest.

■ ACKNOWLEDGEMENTS

We thank the National Health and Medical Research Council (Project Grant 1063786 to S.M. and P.J.S.). C.M.O. holds a Canada Research Chair in Protease Proteomics and Systems Biology and the work was supported by a Canadian Institutes of Health Research grant (MOP-37937) to C.M.O., by the British Columbia Proteomics Network (C.M.O.) and the Canada Foundation for Innovation (C.M.O.). We thank Dr Siew Chai and Peta Burns from Monash University for the kind gift of human insulin-regulated aminopeptidase (IRAP), and Professor James Rini from the University of Toronto, for the stably transfected HEK293S GnT1^{-} cell line. The Australian Red Cross Blood Service is gratefully acknowledged for the provision of human blood for *in vitro* cultivation of *P. falciparum* lines.

■ ABBREVIATIONS USED

Pf-M1, *Plasmodium falciparum* M1 aminopeptidase; *Pf*-M17, *Plasmodium falciparum* M17 aminopeptidase; *Pv*-M1, *Plasmodium vivax* M1 aminopeptidase; *Pv*-M17, *Plasmodium vivax* M17

aminopeptidase; MMP, matrix metalloproteinase; APN, aminopeptidase N; IRAP, insulin-regulated aminopeptidase; FCC, flash column chromatography.

■ REFERENCES

1. *World malaria report*; CC BY-NC-SA 3.0 IGO; World Health Organization: Geneva, Switzerland, 2017.
2. Price, R. N.; Tjitra, E.; Guerra, C. A.; Yeung, S.; White, N. J.; Anstey, N. M. Vivax malaria: Neglected and not benign. *Am. J. Trop. Med. Hyg.* **2007**, 77, 79-87.
3. Sutherland, C. J.; Lansdell, P.; Sanders, M.; Muwanguzi, J.; van Schalkwyk, D. A.; Kaur, H.; Nolder, D.; Tucker, J.; Bennett, H. M.; Otto, T. D.; Berriman, M.; Patel, T. A.; Lynn, R.; Gkrania-Klotsas, E.; Chiodini, P. L. pfk13-Independent treatment failure in four imported cases of *Plasmodium falciparum* malaria treated with artemether-lumefantrine in the united kingdom. *Antimicrob. Agents Chemother.* **2017**, 61.
4. Ashley, E. A.; Dhorda, M.; Fairhurst, R. M.; Amaratunga, C.; Lim, P.; Suon, S.; Sreng, S.; Anderson, J. M.; Mao, S.; Sam, B.; Sopha, C.; Chuor, C. M.; Nguon, C.; Sovannaroth, S.; Pukrittayakamee, S.; Jittamala, P.; Chotivanich, K.; Chutasmit, K.; Suchatsoonthorn, C.; Runcharoen, R.; Hien, T. T.; Thuy-Nhien, N. T.; Thanh, N. V.; Phu, N. H.; Htut, Y.; Han, K. T.; Aye, K. H.; Mokuolu, O. A.; Olaosebikan, R. R.; Folaranmi, O. O.; Mayxay, M.; Khanthavong, M.; Hongvanthong, B.; Newton, P. N.; Onyamboko, M. A.; Fanello, C. I.; Tshefu, A. K.; Mishra, N.; Valecha, N.; Phyo, A. P.; Nosten, F.; Yi, P.; Tripura, R.; Borrmann, S.; Bashraheil, M.; Peshu, J.; Faiz, M. A.; Ghose, A.; Hossain, M. A.; Samad, R.; Rahman, M. R.; Hasan, M. M.; Islam, A.; Miotto, O.; Amato, R.; MacInnis, B.; Stalker, J.; Kwiatkowski, D. P.; Bozdech, Z.; Jeeyapant, A.; Cheah, P. Y.; Sakulthaew, T.; Chalk, J.; Intharabut, B.; Silamut, K.; Lee, S. J.; Vihokhern, B.; Kunasol, C.; Imwong, M.; Tarning, J.; Taylor, W. J.; Yeung, S.; Woodrow, C. J.; Flegg, J. A.; Das, D.; Smith, J.; Venkatesan, M.; Plowe, C. V.; Stepniewska, K.; Guerin, P. J.;

Dondorp, A. M.; Day, N. P.; White, N. J. Spread of artemisinin resistance in *Plasmodium falciparum* malaria. *N. Engl. J. Med.* **2014**, 371, 411-423.

5. Liu, J.; Istvan, E. S.; Gluzman, I. Y.; Gross, J.; Goldberg, D. E. *Plasmodium falciparum* ensures its amino acid supply with multiple acquisition pathways and redundant proteolytic enzyme systems. *Proc. Natl. Acad. Sci. U. S. A.* **2006**, 103, 8840-8845.
6. Loria, P.; Miller, S.; Foley, M.; Tilley, L. Inhibition of the peroxidative degradation of haem as the basis of action of chloroquine and other quinoline antimalarials. *Biochem. J.* **1999**, 339, 363-370.
7. Harbut, M. B.; Velmourougane, G.; Dalal, S.; Reiss, G.; Whisstock, J. C.; Onder, O.; Brisson, D.; McGowan, S.; Klemba, M.; Greenbaum, D. C. Bestatin-based chemical biology strategy reveals distinct roles for malaria M1-and M17-family aminopeptidases. *Proc. Natl. Acad. Sci. U. S. A.* **2011**, 108, E526-E534.
8. McGowan, S. Working in concert: The metalloaminopeptidases from *Plasmodium falciparum*. *Curr. Opin. Struct. Biol.* **2013**, 23, 828-835.
9. Dalal, S.; Klemba, M. Roles for two aminopeptidases in vacuolar hemoglobin catabolism in *Plasmodium falciparum*. *J. Biol. Chem.* **2007**, 282, 35978-35987.
10. Skinner-Adams, T. S.; Lowther, J.; Teuscher, F.; Stack, C. M.; Grembecka, J.; Mucha, A.; Kafarski, P.; Trenholme, K. R.; Dalton, J. P.; Gardiner, D. L. Identification of phosphinate dipeptide analog inhibitors directed against the *Plasmodium falciparum* M17 leucine aminopeptidase as lead antimalarial compounds. *J. Med. Chem.* **2007**, 50, 6024-6031.
11. Skinner-Adams, T. S.; Peatey, C. L.; Anderson, K.; Trenholme, K. R.; Krige, D.; Brown, C. L.; Stack, C.; Nsangou, D. M. M.; Mathews, R. T.; Thivierge, K.; Dalton, J. P.; Gardinerd, D. L. The aminopeptidase inhibitor CHR-2863 is an orally bioavailable inhibitor of murine malaria. *Antimicrob. Agents Chemother.* **2012**, 56, 3244-3249.

12. Bounaadja, L.; Schmitt, M.; Albrecht, S.; Mouray, E.; Tarnus, C.; Florent, I. Selective inhibition of PfA-M1, over PfA-M17, by an amino-benzosuberone derivative blocks malaria parasites development *in vitro* and *in vivo*. *Malaria Journal* **2017**, 16.
13. Chaudhary, M.; Singh, V.; Anvikar, A. R.; Sahi, S. Screening and *in vitro* evaluation of potential *Plasmodium falciparum* leucyl aminopeptidase inhibitors. *Current Computer-Aided Drug Design* **2016**, 12, 282-293.
14. Deprez-Poulain, R.; Flipo, M.; Piveteau, C.; Leroux, F.; Dassonneville, S.; Florent, I.; Maes, L.; Cos, P.; Deprez, B. Structure-activity relationships and blood distribution of antiplasmodial aminopeptidase-1 inhibitors. *J. Med. Chem.* **2012**, 55, 10909-10917.
15. Drinkwater, N.; Vinh, N. B.; Mistry, S. N.; Bamert, R. S.; Ruggeri, C.; Holleran, J. P.; Loganathan, S.; Paiardini, A.; Charman, S. A.; Powell, A. K.; Avery, V. M.; McGowan, S.; Scammells, P. J. Potent dual inhibitors of *Plasmodium falciparum* M1 and M17 aminopeptidases through optimization of S1 pocket interactions. *Eur. J. Med. Chem.* **2016**, 110, 43-64.
16. Gonzalez-Bacerio, J.; Fando, R.; del Monte-Martinez, A.; Charli, J. L.; Chavez, M. D. *Plasmodium falciparum* M1-aminopeptidase: A promising target for the development of antimalarials. *Current Drug Targets* **2014**, 15, 1144-1165.
17. Mistry, S. N.; Drinkwater, N.; Ruggeri, C.; Sivaraman, K. K.; Loganathan, S.; Fletcher, S.; Drag, M.; Paiardini, A.; Avery, V. M.; Scammells, P. J.; McGowan, S. Two-pronged attack: Dual inhibition of *Plasmodium falciparum* M1 and M17 metalloaminopeptidases by a novel series of hydroxamic acid-based inhibitors. *J. Med. Chem.* **2014**, 57, 9168-9183.
18. Paiardini, A.; Bamert, R. S.; Kannan-Sivaraman, K.; Drinkwater, N.; Mistry, S. N.; Scammells, P. J.; McGowan, S. Screening the medicines for malaria venture "malaria box" against the *Plasmodium falciparum* aminopeptidases, M1, M17 and M18. *Plos One* **2015**, 10.

19. Ruggeri, C.; Drinkwater, N.; Sivaraman, K. K.; Bamert, R. S.; McGowan, S.; Paiardini, A. Identification and validation of a potent dual inhibitor of the *P. falciparum* M1 and M17 aminopeptidases using virtual screening. *Plos One* **2015**, 10.

20. Sivaraman, K. K.; Paiardini, A.; Sienczyk, M.; Rugger, C.; Oellig, C. A.; Dalton, J. P.; Scammells, P. J.; Drag, M.; McGowan, S. Synthesis and structure-activity relationships of phosphonic arginine mimetics as inhibitors of the M1 and M17 aminopeptidases from *Plasmodium falciparum*. *J. Med. Chem.* **2013**, 56, 5213-5217.

21. Skinner-Adams, T. S.; Stack, C. M.; Trenholme, K. R.; Brown, C. L.; Grembecka, J.; Lowther, J.; Mucha, A.; Drag, M.; Kafarski, P.; McGowan, S.; Whisstock, J. C.; Gardiner, D. L.; Dalton, J. P. *Plasmodium falciparum* neutral aminopeptidases: New targets for anti-malarials. *Trends Biochem. Sci.* **2010**, 35, 53-61.

22. Thivierge, K.; Mathew, R. T.; Nsangou, D. M. M.; Da Silva, F.; Cotton, S.; Skinner-Adams, T. S.; Trenholme, K. R.; Brown, C. L.; Stack, C. M.; Gardiner, D. L.; Dalton, J. P. Anti-malaria drug development targeting the M1 alanyl and M17 leucyl aminopeptidases. *Arkivoc* **2012**, 330-346.

23. Poreba, M.; McGowan, S.; Skinner-Adams, T. S.; Trenholme, K. R.; Gardiner, D. L.; Whisstock, J. C.; To, J.; Salvesen, G. S.; Dalton, J. P.; Drag, M. Fingerprinting the substrate specificity of M1 and M17 aminopeptidases of human malaria, *Plasmodium falciparum*. *PLoS One* **2012**, 7.

24. McGowan, S.; Oellig, C. A.; Birru, W. A.; Caradoc-Davies, T. T.; Stack, C. M.; Lowther, J.; Skinner-Adams, T.; Mucha, A.; Kafarski, P.; Grembecka, J.; Trenholme, K. R.; Buckle, A. M.; Gardiner, D. L.; Dalton, J. P.; Whisstock, J. C. Structure of the *Plasmodium falciparum* M17 aminopeptidase and significance for the design of drugs targeting the neutral exopeptidases. *Proc. Natl. Acad. Sci. U. S. A.* **2010**, 107, 2449-2454.

25. McGowan, S.; Porter, C. J.; Lowther, J.; Stack, C. M.; Golding, S. J.; Skinner-Adams, T. S.; Trenholme, K. R.; Teuscher, F.; Donnelly, S. M.; Grembecka, J.; Mucha, A.; Kafarski, P.;

DeGori, R.; Buckle, A. M.; Gardiner, D. L.; Whisstock, J. C.; Dalton, J. P. Structural basis for the inhibition of the essential *Plasmodium falciparum* M1 neutral aminopeptidase. *Proc. Natl. Acad. Sci. U. S. A.* **2009**, 106, 2537-2542.

26. Stack, C. M.; Lowther, J.; Cunningham, E.; Donnelly, S.; Gardiner, D. L.; Trenholme, K. R.; Skinner-Adams, T. S.; Teuscher, F.; Grembecka, J.; Mucha, A.; Kafarski, P.; Lua, L.; Bell, A.; Dalton, J. P. Characterization of the *Plasmodium falciparum* M17 leucyl aminopeptidase - a protease involved in amino acid regulation with potential for antimalarial drug development. *J. Biol. Chem.* **2007**, 282, 2069-2080.
27. Kuzmic, P.; Elrod, K. C.; Cregar, L. M.; Sideris, S.; Rai, R.; Janc, J. W. High-throughput screening of enzyme inhibitors: Simultaneous determination of tight-binding inhibition constants and enzyme concentration. *Anal. Biochem.* **2000**, 286, 45-50.
28. Murphy, D. J. Determination of accurate K_i values for tight-binding enzyme inhibitors: An in silico study of experimental error and assay design. *Anal. Biochem.* **2004**, 327, 61-67.
29. Velmourougane, G.; Harbut, M. B.; Dalal, S.; McGowan, S.; Oellig, C. A.; Meinhardt, N.; Whisstock, J. C.; Klemba, M.; Greenbaum, D. C. Synthesis of new (-)-bestatin-based inhibitor libraries reveals a novel binding mode in the S1 pocket of the essential malaria M1 metalloaminopeptidase. *J. Med. Chem.* **2011**, 54, 1655-1666.
30. Lowther, W. T.; Matthews, B. W. Metalloaminopeptidases: Common functional themes in disparate structural surroundings. *Chem. Rev.* **2002**, 102, 4581-4607.
31. Maric, S.; Donnelly, S. M.; Robinsin, M. W.; Skinner-Adams, T.; Trenholme, K. R.; Gardiner, D. L.; Dalton, J. P.; Stack, C. M.; Lowther, J. The M17 leucine aminopeptidase of the malaria parasite *Plasmodium falciparum*: Importance of active site metal ions in the binding of substrates and inhibitors. *Biochemistry* **2009**, 48, 5435-5439.
32. Drinkwater, N.; McGowan, S. From crystal to compound: Structure-based antimalarial drug discovery. *Biochem. J.* **2014**, 461, 349-369.

33. Kyrieleis, O. J. P.; Goettig, P.; Kiefersauer, R.; Huber, R.; Brandstetter, H. Crystal structures of the tricorn interacting factor F3 from thermoplasma acidophilum, a zinc aminopeptidase in three different conformations. *J. Mol. Biol.* **2005**, 349, 787-800.

34. Papakyriakou, A.; Stratikos, E. The role of conformational dynamics in antigen trimming by intracellular aminopeptidases. *Front. Immunol.* **2017**, 8.

35. Overall, C. M.; Kleifeld, O. Towards third generation matrix metalloproteinase inhibitors for cancer therapy. *Br. J. Cancer* **2006**, 94, 941-946.

36. Overall, C. M.; Kleifeld, O. Validating matrix metalloproteinases as drug targets and anti-targets for cancer therapy. *Nat. Rev. Cancer* **2006**, 6, 227-239.

37. Overall, C. M.; Lopez-Otin, C. Strategies for MMP inhibition in cancer: Innovations for the post-trial era. *Nat. Rev. Cancer* **2002**, 2, 657-672.

38. Hitzerd, S. M.; Verbrugge, S. E.; Ossenkoppele, G.; Jansen, G.; Peters, G. J. Positioning of aminopeptidase inhibitors in next generation cancer therapy. *Amino Acids* **2014**, 46, 793-808.

39. Oldfield, E.; Feng, X. X. Resistance-resistant antibiotics. *Trends Pharmacol. Sci.* **2014**, 35, 664-674.

40. Verlinden, B. K.; Louw, A.; Birkholtz, L. M. Resisting resistance: Is there a solution for malaria? *Expert Opin. Drug Discov.* **2016**, 11, 395-406.

41. Wong, A. H. M.; Zhou, D. X.; Rini, J. M. The X-ray crystal structure of human aminopeptidase N reveals a novel dimer and the basis for peptide processing. *J. Biol. Chem.* **2012**, 287, 36804-36813.

42. Butterworth, P. J. The use of Dixon plots to study enzyme inhibition. *Biochim Biophys Acta* **1972**, 289, 251-253.

43. Drinkwater, N.; Bamert, R. S.; Sivaraman, K. K.; Paiardini, A.; McGowan, S. X-ray crystal structures of an orally available aminopeptidase inhibitor, Tosedostat, bound to anti-malarial drug targets PfA-M1 and PfA-M17. *Proteins* **2015**, 83, 789-795.

44. Cowieson, N. P.; Aragao, D.; Clift, M.; Ericsson, D. J.; Gee, C.; Harrop, S. J.; Mudie, N.; Panjikar, S.; Price, J. R.; Riboldi-Tunnicliffe, A.; Williamson, R.; Caradoc-Davies, T. MX1: A bending-magnet crystallography beamline serving both chemical and macromolecular crystallography communities at The Australian Synchrotron. *J. Synchrot. Radiat.* **2015**, 22, 187-190.

45. Battye, T. G. G.; Kontogiannis, L.; Johnson, O.; Powell, H. R.; Leslie, A. G. W. iMosflm: A new graphical interface for diffraction-image processing with mosflm. *Acta Crystallogr. Sect. D-Struct. Biol.* **2011**, 67, 271-281.

46. Kabsch, W. XDS. *Acta Crystallogr. Sect. D-Struct. Biol.* **2010**, 66, 125-132.

47. Evans, P. R.; Murshudov, G. N. How good are my data and what is the resolution? *Acta Crystallogr. D.* **2013**, 69, 1204-1214.

48. Winn, M. D.; Ballard, C. C.; Cowtan, K. D.; Dodson, E. J.; Emsley, P.; Evans, P. R.; Keegan, R. M.; Krissinel, E. B.; Leslie, A. G. W.; McCoy, A.; McNicholas, S. J.; Murshudov, G. N.; Pannu, N. S.; Potterton, E. A.; Powell, H. R.; Read, R. J.; Vagin, A.; Wilson, K. S. Overview of the CCP4 suite and current developments. *Acta Crystallogr. Sect. D-Struct. Biol.* **2011**, 67, 235-242.

49. McCoy, A. J.; Grosse-Kunstleve, R. W.; Adams, P. D.; Winn, M. D.; Storoni, L. C.; Read, R. J. Phaser crystallographic software. *J. Appl. Crystallogr.* **2007**, 40, 658-674.

50. Adams, P. D.; Afonine, P. V.; Bunkoczi, G.; Chen, V. B.; Davis, I. W.; Echols, N.; Headd, J. J.; Hung, L.-W.; Kapral, G. J.; Grosse-Kunstleve, R. W.; McCoy, A. J.; Moriarty, N. W.; Oeffner, R.; Read, R. J.; Richardson, D. C.; Richardson, J. S.; Terwilliger, T. C.; Zwart, P. H. Phenix: A comprehensive python-based system for macromolecular structure solution. *Acta Crystallogr. Sect. D-Struct. Biol.* **2010**, 66, 213-221.

51. Emsley, P.; Cowtan, K. Coot: Model-building tools for molecular graphics. *Acta Crystallogr. Sect. D-Struct. Biol.* **2004**, 60, 2126-2132.

52. Emsley, P.; Lohkamp, B.; Scott, W. G.; Cowtan, K. Features and development of Coot. *Acta Crystallogr. Sect. D-Struct. Biol.* **2010**, 66, 486-501.

53. Duffy, S.; Avery, V. M. Development and optimization of a novel 384-well anti-malarial imaging assay validated for high-throughput screening. *Am. J. Trop. Med. Hyg.* **2012**, 86, 84-92.

SCHEMES

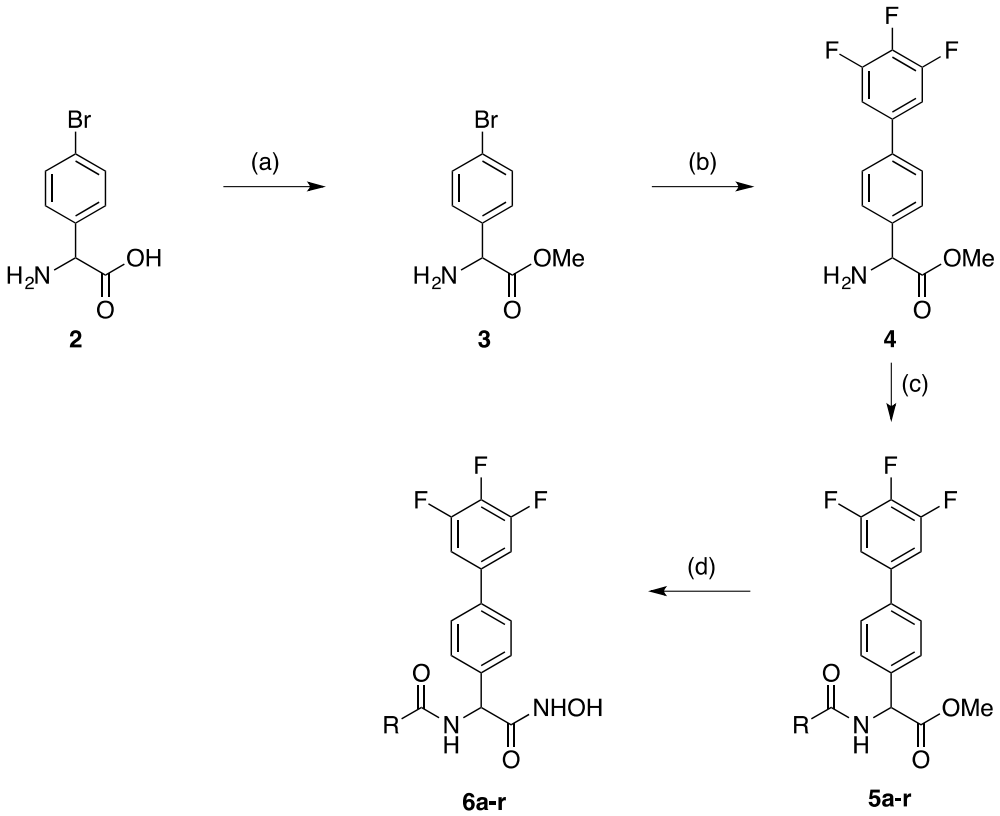

Scheme 1. [a] Reagents and conditions: (a) cat. concd H_2SO_4, MeOH, reflux, 30 h; (b) cat. $PdCl_2(PPh_3)_2$, 3,4,5-trifluorophenylboronic acid, degassed 1M $Na_2CO_{3\,(aq)}$, degassed THF, reflux, 2 h; (c) *Method A*: acid chloride, Et_3N, CH_2Cl_2, rt, 2 h; *Method B*: acid, HCTU, DIPEA, CH_2Cl_2, DMF, rt, 2 h; *Method C*: acid, EDC.HCl, DMAP, CH_2Cl_2, rt, 16 h; (d) $NH_2OH.HCl$, 5M KOH/MeOH, dry MeOH, rt, 16 h.

Table 1. Inhibition of *Pf*-M1 and *Pf*-M17 by hydroxamic acid compounds **6a-r**. K_i values are the mean of three independent experiments.

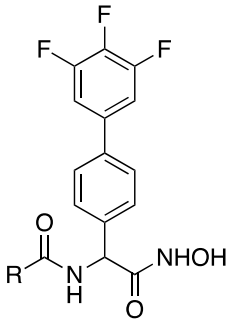

No.	R	K_i (nM) ± S.E.M.			
		Pf-M1	*Pv*-M1	*Pf*-M17	*Pv*-M17
1		331 ± 12	14.1 ± 1.0	147 ± 5	74.8 ± 10.8
6a		417 ± 92	38.9 ± 4.7	426 ± 44	325 ± 31
6b		913 ± 35	66.3 ± 2.9	158 ± 11	108 ± 14
6c	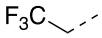	537 ± 44	149 ± 5	999 ± 112	1050 ± 30
6d-a	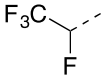 (±)-*R,R*	257 ± 14	11.2 ± 0.6	814 ± 71	382 ± 59
6d-b	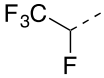 (±)-*R,S*	1489 ± 88	211 ± 33	2190 ± 124	1240 ± 40
6e	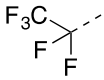	815 ± 72	90.0 ± 10.3	200 ± 19	97.5 ± 6.6
6f		532 ± 19	90.6 ± 8.9	492 ± 26	572 ± 74
6g		236 ± 11	29.8 ± 1.2	185 ± 5	371 ± 58
6h		285 ± 40	13.1 ± 0.8	300 ± 24	336 ± 30
6i		818 ± 45	37.6 ± 5.1	195 ± 11	178 ± 19

6j	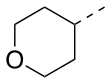	431 ± 10	159 ± 6	290 ± 28	494 ± 46
6k		137 ± 11	122 ± 17	28.9 ± 4.4	18.6 ± 3.9
6l		269 ± 12	6.39 ± 0.62	101 ± 11	3.60 ± 0.97
6m	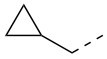	202 ± 27	17.9 ± 0.5	270 ± 8	303 ± 40
6n	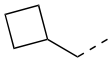	177 ± 8	2.85 ± 0.66	306 ± 30	75.6 ± 12.4
6o	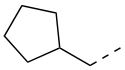	216 ± 12	7.58 ± 0.83	138 ± 9	211 ± 19
6p	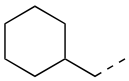	812 ± 64	13.2 ± 1.0	288 ± 5	148 ± 17
6q		88.9 ± 7.2	1.73 ± 0.15	318 ± 33	77.9 ± 18.1
6r	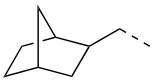	136 ± 14	12.7 ± 0.5	127 ± 12	93.1 ± 8.2

Table 2. Inhibition of resistant *P. falciparum* strains by key compounds

Cpd	IC_{50} (nM) ± SD		CC_{50} (nM) ± SD	% Inhibition of HEK293 cells at		Selectivity Index[c]
	Pf-3D7	*Pf-Dd2*	HEK293[a]	10 μM	40 μM[b]	
Artesunate	1.6 ± 0.5	1.0 ± 0.3	-	42.3 ± 3.5	-	
Chloroquine	11.7 ± 3.5	90.3 ± 29.0	-	17.3 ± 2.8	57.0 ± 8.6	≥ 1709
DHA	0.5 ± 0.1	0.4 ± 0.3	-	31.0 ± 6.0	-	
Puromycin	110.8 ± 101.2	106.6 ± 100.9	500.1 ± 69.3	104.9 ± 2.9	104.9 ± 3.0	4.5
Pyrimethamine	5.1 ± 3.2	NI		34.4 ± 6.4	53.7 ± 6.8	≥ 1960
Pyronaridine	7.0 ± 6.0	7.9 ± 5.5	3549.5 ±272.2	102.0 ± 3.1	95.6 ± 6.4	507
1	83.1 ± 16.1	81.7 ± 6.8	-	1.1 ± 0.6	80.7 ± 11.7	≥ 241
6g	126.5 ± 31.8	120.2 ± 26.6	-	6.0 ± 1.1	48.2 ± 5.3	≥ 158
6k	356.9 ± 49.9	312.8 ± 110.2	-	2.1 ± 0.5	42.9 ± 23.2	≥ 56
6l	14.6 ± 0.8	13.8 ± 0.5	-	4.8 ± 2.2	98.4 ± 2.6	≥ 1370
6m	135.8 ± 11.5	108.8 ± 0.5	-	6.4 ± 2.4	37.6 ± 7.9	-
6n	55.4 ± 4.2	29.2 ± 3.5	-	6.3 ± 1.9	5.6 ± 2.3	-
6o	168.3 ± 27.6	124.7 ± 4.5	-	3.1 ± 1.8	-1.0 ± 2.0	-
6q	76.8 ± 22.1	24.1 ± 3.6	-	10.4 ± 0.5	82.4 ± 10.4	≥ 260
6r	219.5 ± 40.2	120.1 ± 0.7	-	0.6 ± 0.3	19.7 ± 38.9	-

[a] CC_{50} values could not be calculated for compounds with inhibition not reaching 50% at 40 μM, or whose dose-response curve did not reach full inhibition plateau at the tested concentration range.

[b] Artesunate and DHA were tested at 10 μM top concentration.

[c] Actual SI values calculated by CC_{50}/IC_{50} (puromycin and pyronaridine). Approximate SI values (indicated by ≥) calculated by assuming that compounds showing 51-100 % inhibition at 40 μM would have a CC_{50} of ≥ 20 μM.

FIGURES AND FIGURE LEGENDS.

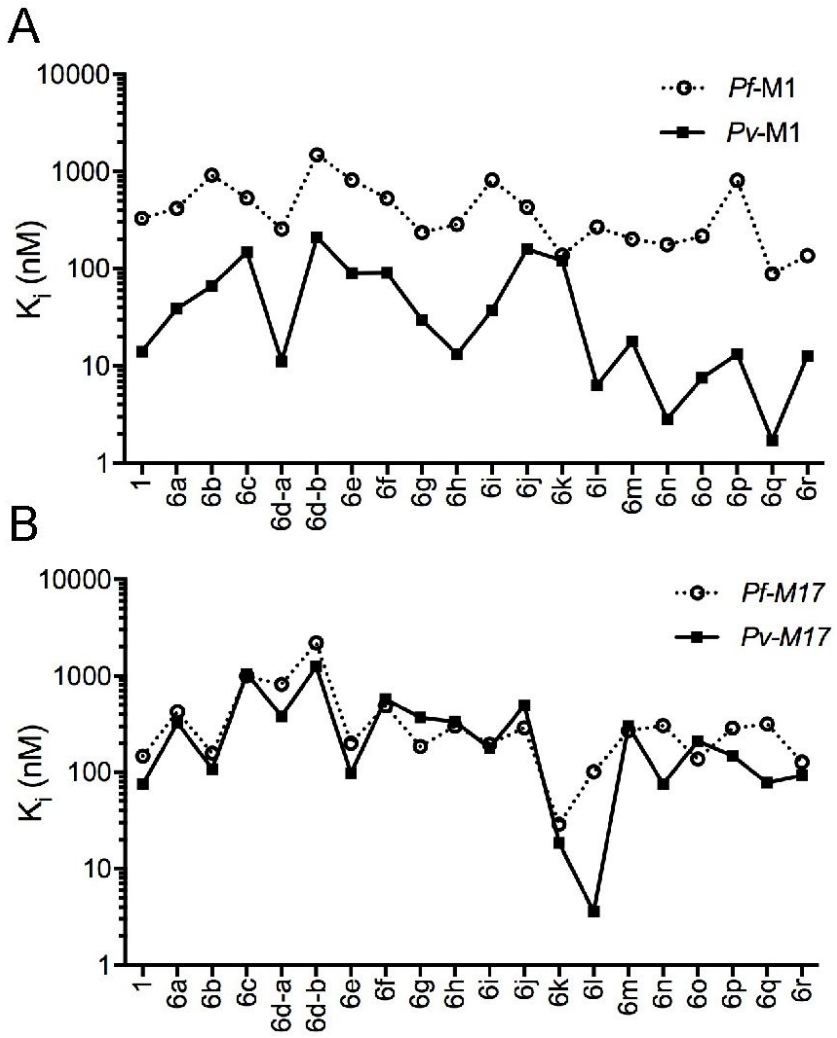

Figure 1. Compound inhibition trends for (A) *Pf*- and *Pv*- M1 enzymes, and (B) *Pf*- and *Pv*- M17 aminopeptidases.

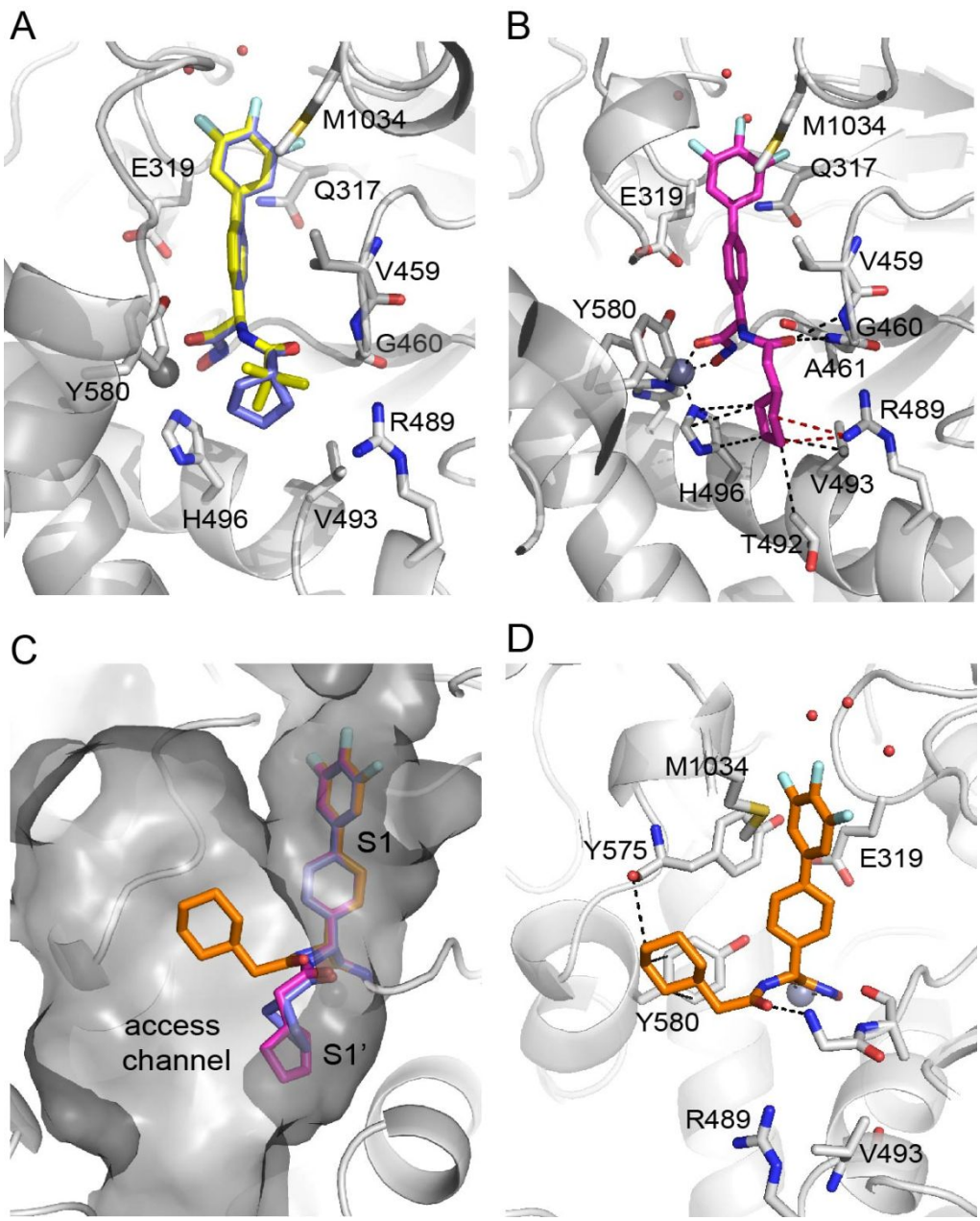

Figure 2. Binding mode of selected compounds to *Pf*-M1 (grey cartoon). (A) Overlay of the binding position of **1** (yellow sticks) and **6h** (blue sticks) in the *Pf*-M1 binding pocket (grey sticks). (B) Structure of **6o** in complex with *Pf*-M1 (grey sticks). Molecular interactions between **6o** and the S1' subsite are indicated by dashed lines. (C) Solvent accessible surface of *Pf*-M1 (grey) with the S1 and S1' subsites as well as the substrate/product access channel are indicated. Stick representation shows the binding positions of **6h** (purple), **6o** (pink), and **6p** (orange). (D) Structure of **6p** (orange) in complex with *Pf*-M1 (grey sticks). Molecular interactions between the N-acyl and ethyl-linked cyclohexane moieties of **6o** are indicated by dashed lines.

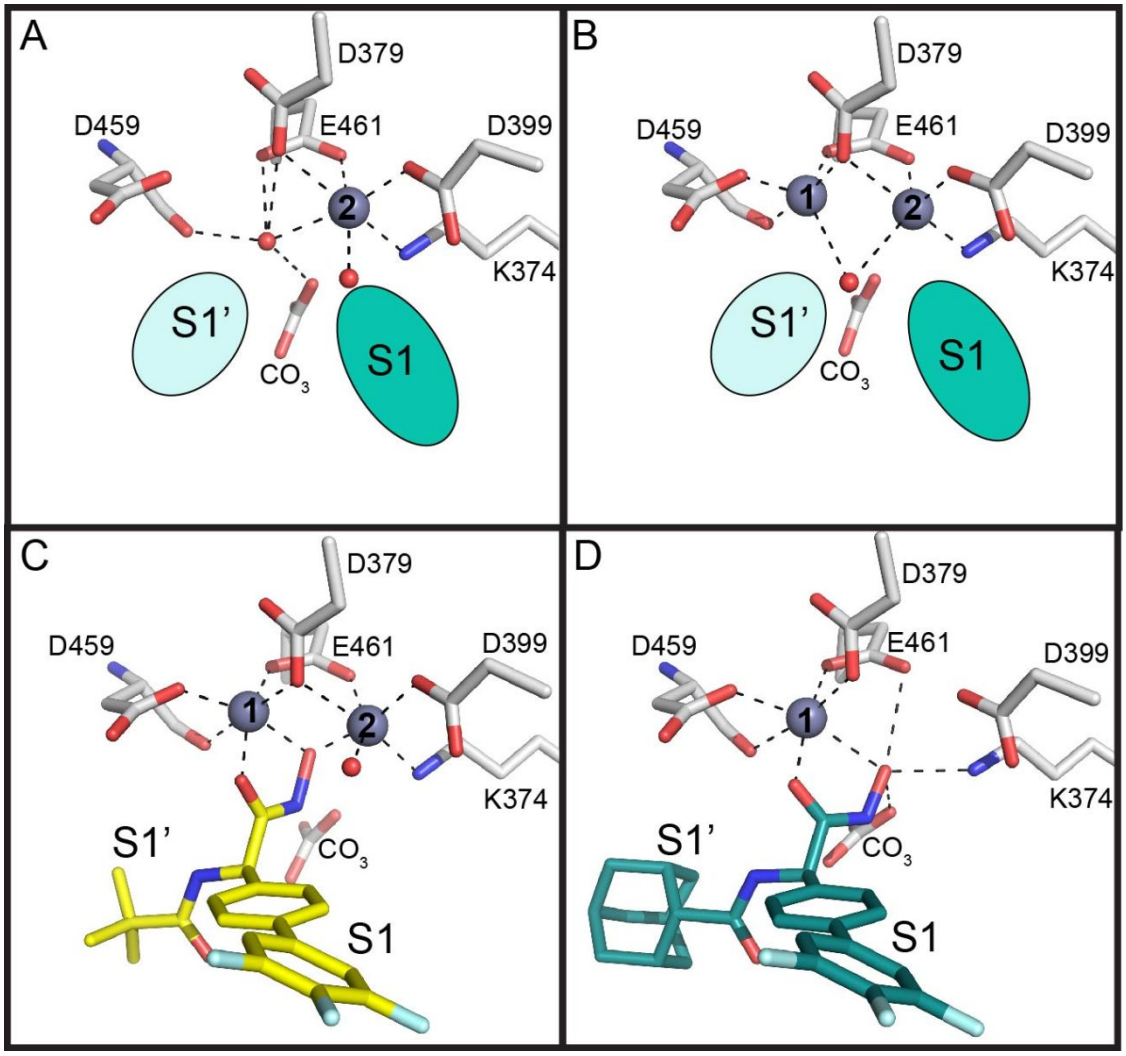

Figure 3. Arrangement of the binuclear metal site of *Pf*-M17 (grey sticks and spheres) with S1 and S1' substrate binding sites and catalytic carbonate ion indicated. (A) Crystal structure of *Pf*-M17 with only the catalytic metal site occupied (Zn^{2+}, site 2).[24] (B) *Pf*-M17 crystals treated with a Zn^{2+} soak solution yield a structure with both the regulatory site 1 and catalytic site 2 occupied by Zn^{2+}.[24] (C) Compound **1** (yellow) coordinates both Zn^{2+} ions through the hydroxamic acid moiety.[15] (D) Compound **6k** (teal) displaces the catalytic Zn^{2+} from site 2 of *Pf*-M17.

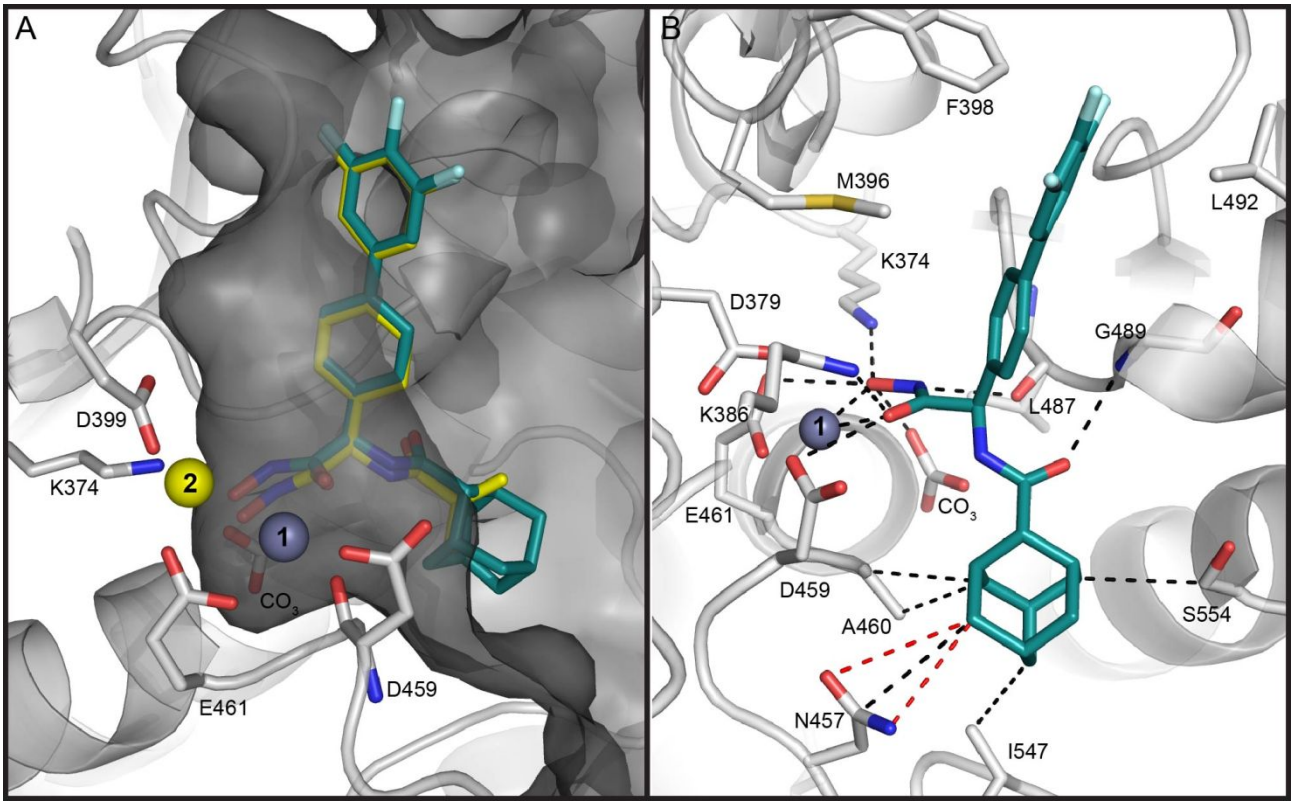

Figure 4. Binding mode of selected compounds to *Pf*-M17. (A) Solvent accessible surface of *Pf*-M17 (grey) with catalytic Zn^{2+} (site 2, yellow) and regulatory Zn^{2+} (site 1, grey) indicated. Stick representation shows the binding positions of **1** (yellow) and **6k** (teal). Zn^{2+} occupies site 2 (yellow) when *Pf*-M17 is in complex with **1** but not in complex with **6k**. (B) Structure of **6k** in complex with *Pf*-M17 (grey sticks). Molecular interactions between **6k** (teal) and the site 1 Zn^{2+} and S1' subsite are indicated by dashed lines.

TABLE OF CONTENTS GRAPHIC

Proposed role of aminopeptidases in plasmodial hemoglobin digestion pathway and mechanism of hydroxamate inhibitor series described herein.

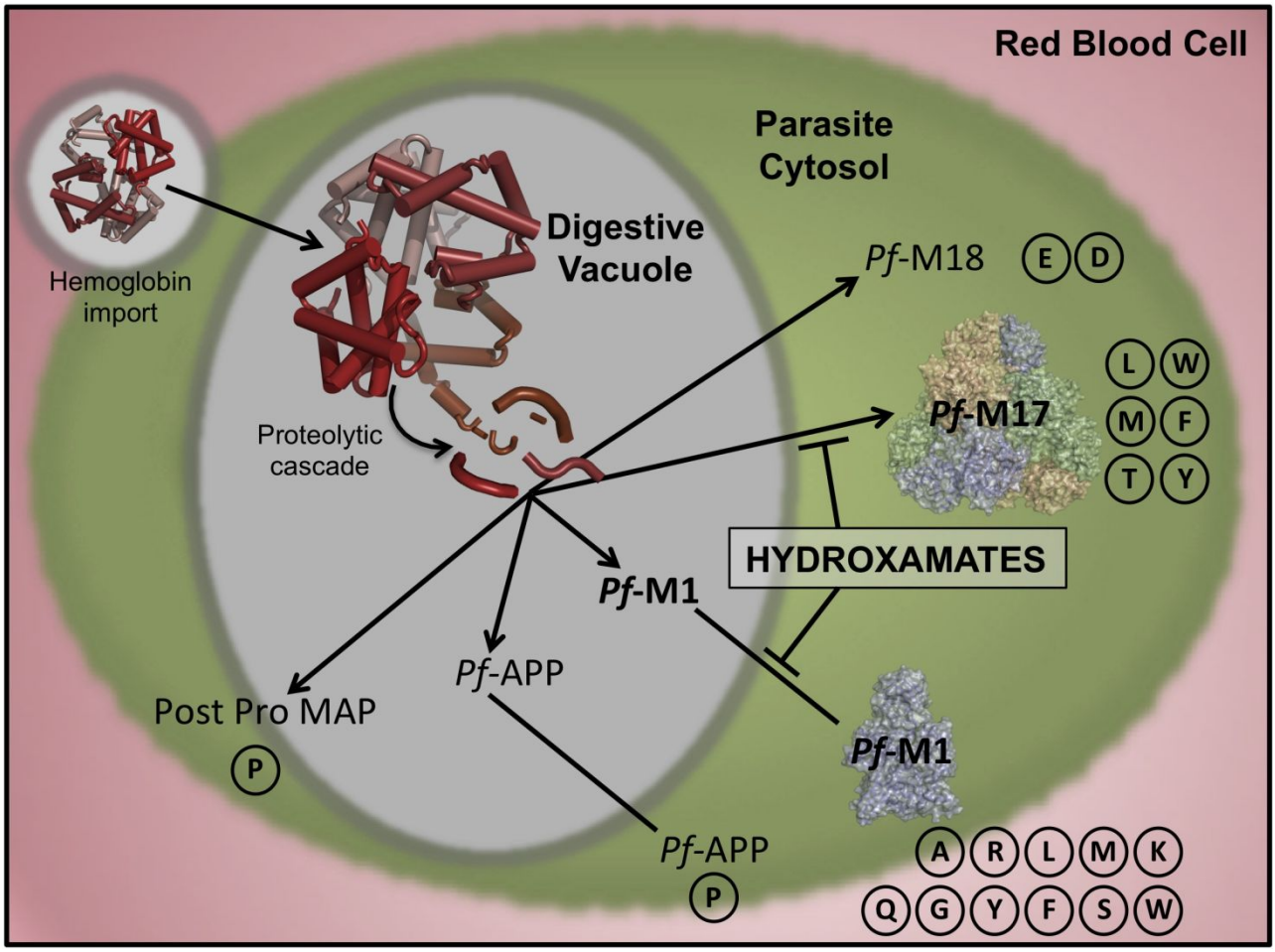

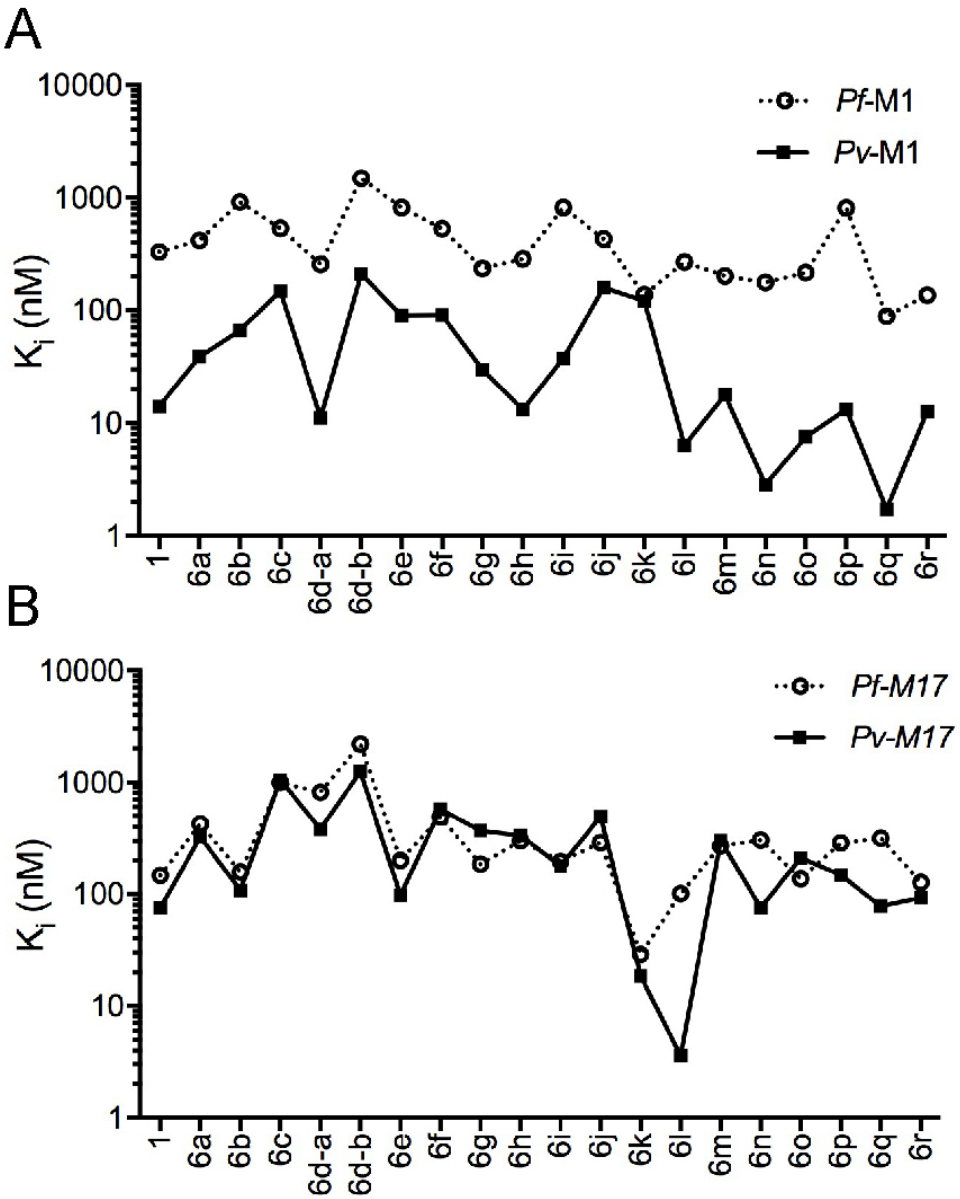

Figure 1. Compound inhibition trends for (A) Pf- and Pv- M1 enzymes, and (B) Pf- and Pv- M17 aminopeptidases.

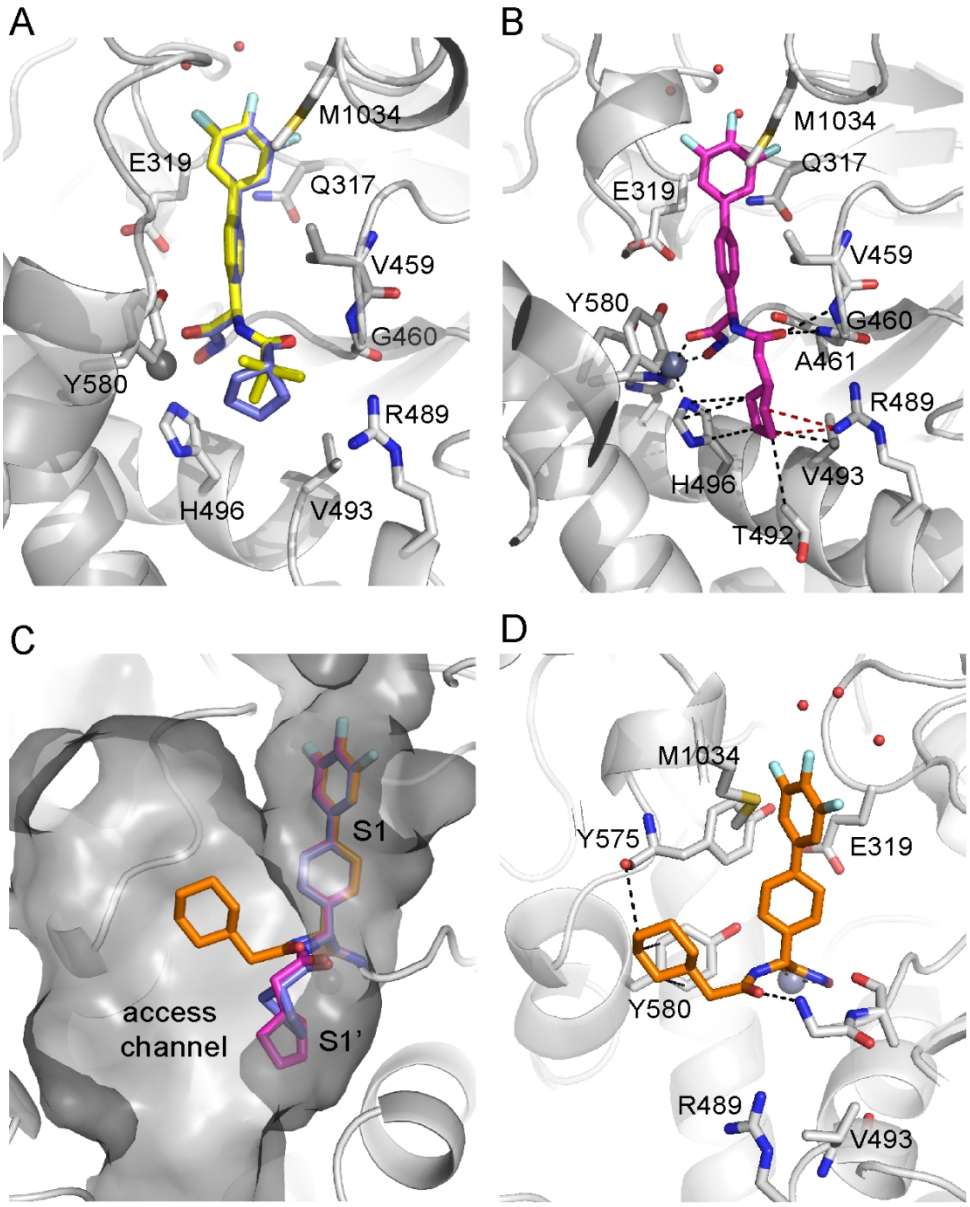

Figure 2. Binding mode of selected compounds to Pf-M1 (grey cartoon). (A) Overlay of the binding position of 1 (yellow sticks) and 6h (blue sticks) in the Pf-M1 binding pocket (grey sticks). (B) Structure of 6o in complex with Pf-M1 (grey sticks). Molecular interactions between 6o and the S1′ subsite are indicated by dashed lines. (C) Solvent accessible surface of Pf-M1 (grey) with the S1 and S1′ subsites as well as the substrate/product access channel are indicated. Stick representation shows the binding positions of 6h (purple), 6o (pink), and 6p (orange). (D) Structure of 6p (orange) in complex with Pf-M1 (grey sticks). Molecular interactions between the N-acyl and ethyl-linked cyclohexane moieties of 6o are indicated by dashed lines.

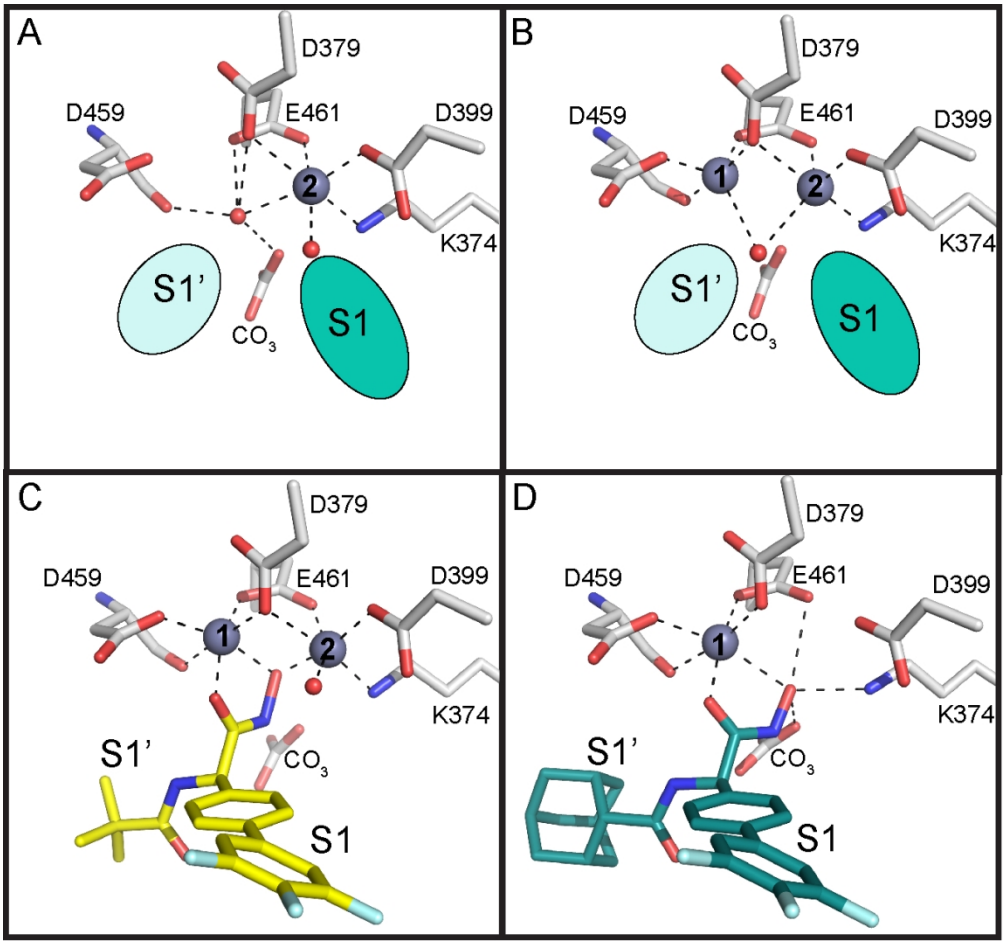

Figure 3. Arrangement of the binuclear metal site of Pf-M17 (grey sticks and spheres) with S1 and S1' substrate binding sites and catalytic carbonate ion indicated. (A) Crystal structure of Pf-M17 with only the catalytic metal site occupied (Zn2+, site 2).24 (B) Pf-M17 crystals treated with a Zn2+ soak solution yield a structure with both the regulatory site 1 and catalytic site 2 occupied by Zn2+.24 (C) Compound 1 (yellow) coordinates both Zn2+ ions through the hydroxamic acid moiety.15 (D) Compound 6k (teal) displaces the catalytic Zn2+ from site 2 of Pf-M17.

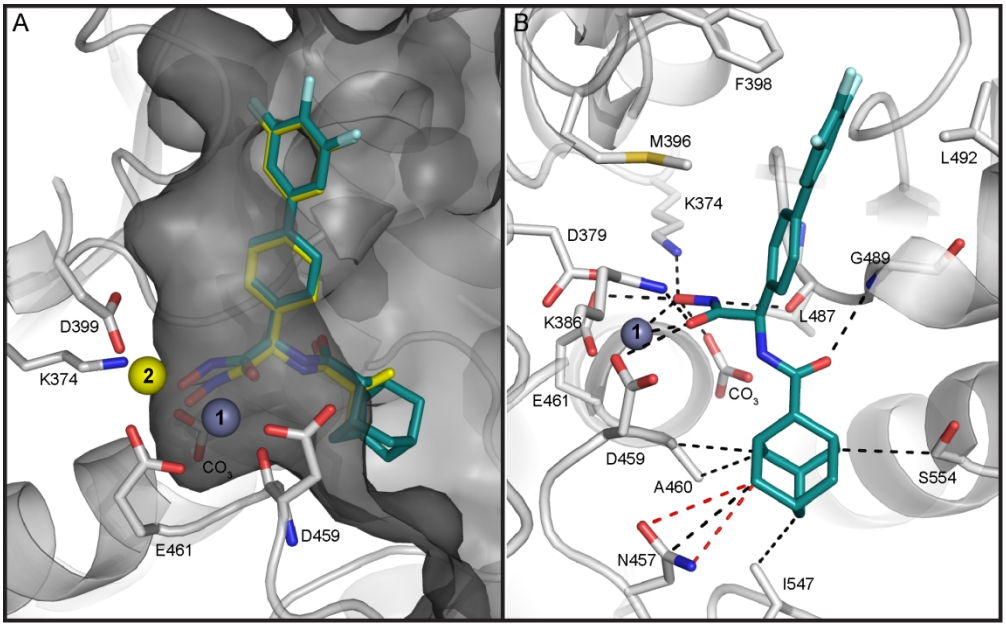

Figure 4. Binding mode of selected compounds to Pf-M17. (A) Solvent accessible surface of Pf-M17 (grey) with catalytic Zn2+ (site 2, yellow) and regulatory Zn2+ (site 1, grey) indicated. Stick representation shows the binding positions of 1 (yellow) and 6k (teal). Zn2+ occupies site 2 (yellow) when Pf-M17 is in complex with 1 but not in complex with 6k. (B) Structure of 6k in complex with Pf-M17 (grey sticks). Molecular interactions between 6k (teal) and the site 1 Zn2+ and S1′ subsite are indicated by dashed lines.

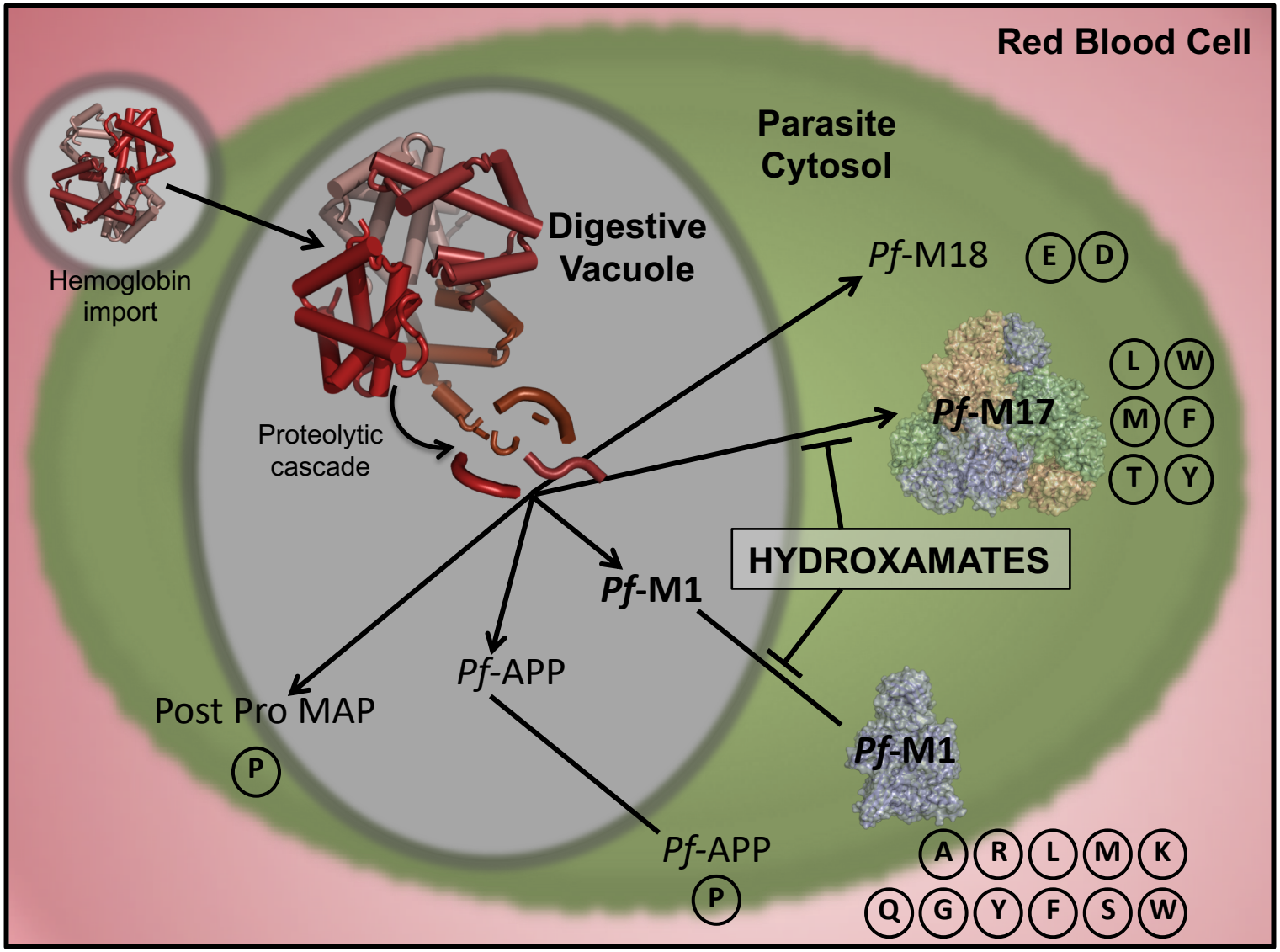
Red Blood Cell
Parasite Cytosol
Digestive Vacuole
Hemoglobin import
Proteolytic cascade
Pf-M18
E D
Pf-M17
L W
M F
T Y
HYDROXAMATES
Pf-M1
Pf-APP
Post Pro MAP
P
Pf-M1
Pf-APP
P
A R L M K
Q G Y F S W